รายงานวิจัยฉบับสมบูรณ์

โครงการ การสังเคราะห์และสมบัติทางไฟฟ้าของสารประกอบเทลลูเรียมออกไซด์ไพโรคลอที่นำไฟฟ้าได้

โดย ผู้ช่วยศาสตราจารย์ ดร.ธีรนันท์ ศิริตานนท์
สาขาวิชาเคมี สำนักวิชาวิทยาศาสตร์
มหาวิทยาลัยเทคโนโลยีสุรนารี

มกราคม 2560

สัญญาเลขที่ TRG5780068

รายงานวิจัยฉบับสมบูรณ์

โครงการการสังเคราะห์และสมบัติทางไฟฟ้าของสารประกอบเทลลูเรียมออกไซด์ไพโรคลอที่นำไฟฟ้าได้

ผู้ช่วยศาสตราจารย์ ดร.ธีรนันท์ ศิริตานนท์
สาขาวิชาเคมี สำนักวิชาวิทยาศาสตร์
มหาวิทยาลัยเทคโนโลยีสุรนารี

สนับสนุนโดยสำนักงานกองทุนสนับสนุนการวิจัยและ
มหาวิทยาลัยเทคโนโลยีสุรนารี

กิตติกรรมประกาศ

This work is financially supported by the Thailand Research Fund and Suranaree University of Technology. In addition, contributions from several people and organizations have allowed this work to be completed. Their supports are greatly appreciated.

In addition to all co-authors of the manuscript whose contributions are appreciated, I would like to thank Assoc. Prof. Sirichok Jungthawan for useful suggestions and discussions on the calculations. The synchrotron light research institute (public organization), Thailand, especially SUT-NANOTEC-SLRI joint research facility, is acknowledged for XPS facilities.

Abstract

Project Code : TRG5780068

Project Title : Synthesis and electrical properties of conducting tellurium oxide pyrochlores

Investigator : Assist. Prof. Dr. Theeranun Siritanon
School of Chemistry, Institute of Science,
Suranaree University of Technology

E-mail Address : theeranun@sut.ac.th

Project Period : 2 years

The preparation and electronic properties of $Cs_{1-x}A_xAl_{0.33}Te_{1.67}O_6$ (A = K, Rb, and Cs) are reported. Replacing Cs with smaller Rb and K reduces cell parameters of the compounds but does not affect the overall structure. Electronic conductivity of all samples were measured and explained based on the band conduction model. Although XPS $Te3d_{5/2}$ spectra indicate that all samples contain similar amount of Te^{4+}/Te^{6+} mixed valency, their conductivity is varied from about 0.1 Scm in $CsAl_{0.33}Te_{1.67}O_6$ to 3 x 10^{-5}Scm in $RbAl_{0.33}Te_{1.67}O_6$ and 3 x 10^{-7}Scm in $KAl_{0.33}Te_{1.67}O_6$ at 300K. To explain such large differences, the band structure diagrams are proposed based on the UV-Vis spectra and XPS spectra at valence band region. When the obtained activation energy of conduction and the proposed band diagram are considered, it is concluded that $AAl_{0.33}Te_{1.67}O_6$ (A = K, Rb, and Cs) are n-type semiconductors. The defect levels in these samples originate from Te^{4+} whose energy level relative to the conduction band minimum is different from samples to samples. Such differences are affected by Cs content in the structure as Cs seems to lower the band gap energy and increase the valence band maximum. It is the position of these defect levels that determines the electronic conductivity of the compounds.

Keywords : Pyrochlores, oxides, electronic properties, X-ray photoelectron spectroscopy

บทคัดย่อ

รหัสโครงการ : TRG5780068

ชื่อโครงการ : การสังเคราะห์และสมบัติทางไฟฟ้าของสารประกอบเทลลูเรียมออกไซด์ไพโรคลอที่นำไฟฟ้าได้

ชื่อนักวิจัย : Assist. Prof. Dr. Theeranun Siritanon
School of Chemistry, Institute of Science,
Suranaree University of Technology

E-mail Address : theeranun@sut.ac.th

ระยะเวลาโครงการ : 2 years

โครงการวิจัยนี้รายงานการเตรียมและสมบัติทางไฟฟ้าของ $Cs_{1-x}A_xAl_{0.33}Te_{1.67}O_6$ (A = K, Rb, and Cs) โดยพบว่าการแทนที่ Cs ด้วย Rb และ K ซึ่งมีขนาดเล็กกว่าไม่ส่งผลทำให้โครงสร้างเปลี่ยนแปลง นอกจากนี้ยังศึกษาสมบัติทางไฟฟ้าของสารและอธิบายสมบัติดังกล่าวโดยอาศัยโครงสร้างแถบพลังงาน (band structure) ทั้งนี้ถึงแม้ว่าการศึกษาด้วยเทคนิคสเปคโตรสโคปีของอนุภาคอิเล็กตรอนที่ถูกปลดปล่อยด้วยรังสีเอกซ์หรือ XPS พบว่าสารตัวอย่างทั้งหมดมีองค์ประกอบของ Te^{4+} และ Te^{6+} ผสมกันอยู่ในปริมาณที่ใกล้เคียงกันแต่การนำฟ้าในสารตัวอย่างกลับมีความแตกต่างกันมากคือสารตัวอย่าง $CsAl_{0.33}Te_{1.67}O_6$ มีความนำไฟฟ้า 0.1 Scm ที่อุณหภูมิห้อง ในขณะที่ $RbAl_{0.33}Te_{1.67}O_6$ และ $KAl_{0.33}Te_{1.67}O_6$ มีความนำไฟฟ้าเพียง 3×10^{-5} Scm และ 3×10^{-7} Scm ตามลำดับเท่านั้น เพื่ออธิบายความแตกต่างดังกล่าวโครงการวิจัยจึงอาศัยผลการทดลองสมบัติการดูดกลืนแสงและ XPS ในการเสนอโครงสร้างแถบพลังงานของสารตัวอย่างขึ้น ซึ่งทำให้อธิบายได้ว่าสารตัวอย่างมีสมบัติเป็นสารกึ่งตัวนำชนิดเอ็นเนื่องจากมีระดับพลังงานเจือ (defect level) ของ Te^{4+} โดยความแตกต่างระหว่างระดับพลังงานเจือนี้กับแถบตัวนำ (conduction band) เป็นตัวกำหนดความสามารถในการนำไฟฟ้าของสารและ Cs ในโครงสร้างมีบทบาททำให้ช่องว่างพลังงาน (band gap energy) ลดลงและตำแหน่งของแถบเวเลนซ์สูงขึ้นซึ่งส่งผลให้ความแตกต่างระหว่างระดับพลังงานเจือกับแถบตัวนำมีค่าต่างกันเมื่อมีปริมาณ Cs ในโครงสร้างต่างกันและทำให้สารตัวอย่างมีความนำไฟฟ้าต่างกันในที่สุด

คำสำคัญ :ไพโรคลอ, ออกไซด์, สมบัติทางไฟฟ้า, สเปคโตรสโคปีของอนุภาคอิเล็กตรอนที่ถูกปลดปล่อยด้วยรังสีเอกซ์

1. Introduction

At temperatures lower than the critical point (T_c), superconductors exhibit several unique properties including having zero resistance and expelling magnetic field (Meissner effect). Such properties allow many applications; some are already available such as the widely used Magnetic Resonance Imaging (MRI), superconducting magnetic energy storage (SMES), and high energy physics accelerator. However, the maximum uses of superconductors are still limited by some factors especially the critical temperatures which are usually much lower than room temperature. Moreover, many high-T_c superconductors have complicate structures which are difficult to prepare and fabricate in large scale. In addition, some materials consist of toxic elements which raises concerns in environmental issues. Nevertheless, the benefits of superconductivity outweigh all the difficulties. As a result, scientists never stop trying to discover better materials and improve the existing ones.

Superconductivity has been observed in many materials including mixed valence oxides with heavy post-transition metals. Sleight et al. reported the superconductivity in $BaBi_{1-x}Pb_xO_3$ perovskites with transition temperatures as high as 13K[1]. Similar phenomenon is found in $BaPb_{1-x}Sb_xO_3$ where the superconductivity was reported with transition temperature of 3.5K by Cava et al.[2] It is reported that diffused s orbitals in Pb, Sb, and Bi play an important role in superconductivity of the mentioned compounds. In addition, Post transition elements form oxides with interesting structures and properties. Several oxides containing heavy post transition elements are known to have good electronic conductivity due to the presence of diffused s orbitals which results in wide conduction bands and low carrier mobility. Some well-known examples include In_2O_3, $ZnSnO_3$, and $In_4Sn_3O_{12}$.[3-5]

As a member of heavy transition elements which also has diffused s orbital, oxides of tellurium are interesting new candidates. Although there is no report on superconductivity in any tellurium oxides, relatively high electronic conductivities have been reported in some tellurium oxides with general formula $Cs(M,Te)_2O_6$; M = 2+, 3+ and 4+ cations which show n-type semiconducting behavior due to Te^{4+}/Te^{6+} mixed valency as summarized in Table 1.[6]

Table 1: $Cs(M,Te)_2O_6$ oxides with pyrochlore structure and their electrical properties

Compound	a (Å)	ρ (Ωcm) @RT	S (mV/K) @RT
$CsM^{3+}_{0.33}Te_{1.67}O_6$			
$Cs(Al_{0.33}Te_{1.67})O_6$	10.085	10	-87
$Cs(Cr_{0.33}Te_{1.67})O_6$	10.159	$>10^6$	-
$Cs(Mn_{0.33}Te_{1.67})O_6$	10.186	$3x10^3$	-390
$Cs(Fe_{0.33}Te_{1.67})O_6$	10.183	42	-130
$Cs(Co_{0.33}Te_{1.67})O_6$	10.175	118	-206
$Cs(Ga_{0.33}Te_{1.67})O_6$	10.158	3	-50
$Cs(Sc_{0.33}Te_{1.67})O_6$	10.256	10^5	-
$Cs(In_{0.33}Te_{1.67})O_6$	10.281	33	-150
$Cs(Tl_{0.33}Te_{1.67})O_6$	10.345	3	-70
$Cs(Lu_{0.33}Te_{1.67}O_6$	10.348	$>10^6$	-
$Cs(Yb_{0.33}Te_{1.67})O_6$	10.357	$>10^6$	-
$Cs(Tm_{0.33}Te_{1.67})O_6$	10.364	$>10^6$	-
$Cs(Er_{0.33}Te_{1.67})O_6$	10.375	$>10^6$	-
$Cs(Ho_{0.33}Te_{1.67})O_6$	10.394	$>10^6$	-
$CsM^{4+}_{0.5}Te_{1.5}O_6$			
$Cs(Ge_{0.5}Te_{1.5})O_6$	10.044	0.5	-51
$Cs(Ti_{0.5}Te_{1.5})O_6$	10.150	$>10^6$	-
$Cs(Rh_{0.5}Te_{1.5})O_6$	10.181	10^3	-90
$CsM^{2+}_{0.25}Te_{1.75}O_6$			
$Cs(Mg_{0.25}Te_{1.75})O_6$	10.220	482	-180
$Cs(Zn_{0.25}Te_{1.75})O_6$	10.233	$>10^6$	-
$Cs(Ni_{0.25}Te_{1.75})O_6$	10.219	$>10^6$	-

It has been established that M cations in the mentioned formula play some roles in determining electronic conductivity of the compounds. Smaller M cations reduce the cell parameter which compress Te^{4+} in the structure and consequently destabilize it. In addition, suitable M cations could provide orbitals with appropriate energy to overlap with Te 5s which could give rise to samples with higher conductivity. Only one compound in these series, $Cs(Al,Te)_2O_6$, was extensively investigated where the presence of Te^{4+} in the octahedral network is detected through detailed structural studies. It was concluded that Te^{4+}/Te^{6+} mixed valency in the compounds is a result of small deviations from stoichiometry[7]. However, the role of Cs in the structure remains unclear. Thus, the objectives of this work are to deepen the understanding of these series of oxides and to study the effects of cations at Cs position on the electronic properties of compounds in $Cs_{1-x}A_xAl_{0.33}Te_{1.67}O_6$; A = Rb and K series. The obtained knowledge is expected to be beneficial to the future studies and designs of conducting metal oxides.

2. Objectives

2.1 To prepare pyrochlore oxides with the general formula $Cs_{1-x}A_xAl_{0.33}Te_{1.67}O_6$; A = Rb and K with x =0, 0.2, 0.4, 0.6, 0.8, and 1

2.2 To study structure, composition, and electronic properties of the obtained compounds

2.3 To explain the relationships between structure, composition, and the electronic properties of the compounds.

3. Experimental and calculational details

3.1 Sample preparations

All samples were prepared by solid state reaction. The reactants are $CsNO_3$ (Sigma-Aldrich, 99+%), $RbNO_3$ (Acros organic, 99.8%), Al_2O_3 (Acros organic, 99+ %, for Rb-doped series), $Al(OH)_3$ (Acros organic, 99.9%, for K-doped series) and TeO_2 (Acros organic, 99+%). Stoichiometric mixtures of the reactants were weighed and ground in an agate mortar and

heated at 500 ^{o}C for 5 h in air. After that, the samples were reground, pressed in to pellets and sintered at 625 ^{o}C for 12 h in air.

3.2 Characterizations

Powder X-ray diffraction (XRD) patterns were recorded by a Bruker D2 Phaser diffractometer (Cu Kα radiation, λ = 1.5406 Å) for phase identification. The X-ray Photoelectron Spectra (XPS) of Cs 3d, Rb 3d, K 2p, Al 1s, O 1s, Te $3d_{5/2}$ and valence band (VB) were recorded by a PHI5000 VersaProbe II XPS instruments (ULVAC-PHI, Japan) (Monochromatic X-ray of Al Kα ,1486.6 eV) at SUT-NANOTEC-SLRI joint research facility, Synchrotron Light Research Institute (SLRI), Thailand. The binding energies drift due to charging effects were corrected using the position of the C 1s as a reference at 284.8 eV.[8-9] Agilent UV-Vis-NIR spectrophotometer modeled Carry 5000 was used for optical diffuse reflectance spectroscopy (DRS). The diffuse reflectance (%R) spectra were recorded in the wavelength range of 200-2000 nm with the double beam mode. Bandgap energy was obtained by extrapolation of the plot of $(Kh\nu)^{1/2}$ versus photon energy ($h\nu$), where K is reflectance transformed according to Kubelka–Munk function [$K = (1 - R)^2/2(R)$], $R = (\%R_{sample}/\%R_{standard})$.[10-11] The Electrical conductivity of all sintered samples was measured from 300 to 673 K by four probe method using Keysight B2901A source/measure unit. In the typical measurements, platinum wires were connected to the sintered piece of the sample using the conducting high-temperature silver paint. The other side of the wires were connected to the source/measure unit while the sample was put in a tube furnace. The temperature was raised to the designated values and the measurements were performed after the equilibrium was reached (the temperatures remained constant). The measured resistance was used, along with dimensions of the sample, to calculate the resistivity.

3.3 Calculations

The density of states (DOS) were calculated based on density functional theory (DFT) using the Vienna ab initio simulation package (VASP)[12-13] mploying the Perdew, Burke, Ernzerhof (PBE) exchange-correlation function[14] implemented with the projector augmented-wave method (PAW).[15-16] Γ-centered 3x3x2 Monkhorst-Pack k-mesh was used for the Brillouin

zone integrations. The cutoff energy for plane-wave basis sets was set at 520 eV. Structural relaxation was performed until the force on each ion is less than 0.01 eV/Å.

4. Results

4.1 X-ray diffractions

Powder X-ray diffraction patterns indicate that all samples are single phase (Fig. 1). All diffractions can be indexed as AB_2O_6 defect cubic pyrochlore structure (β-pyrochlore) with $Fd\bar{3}m$ space group.[17]

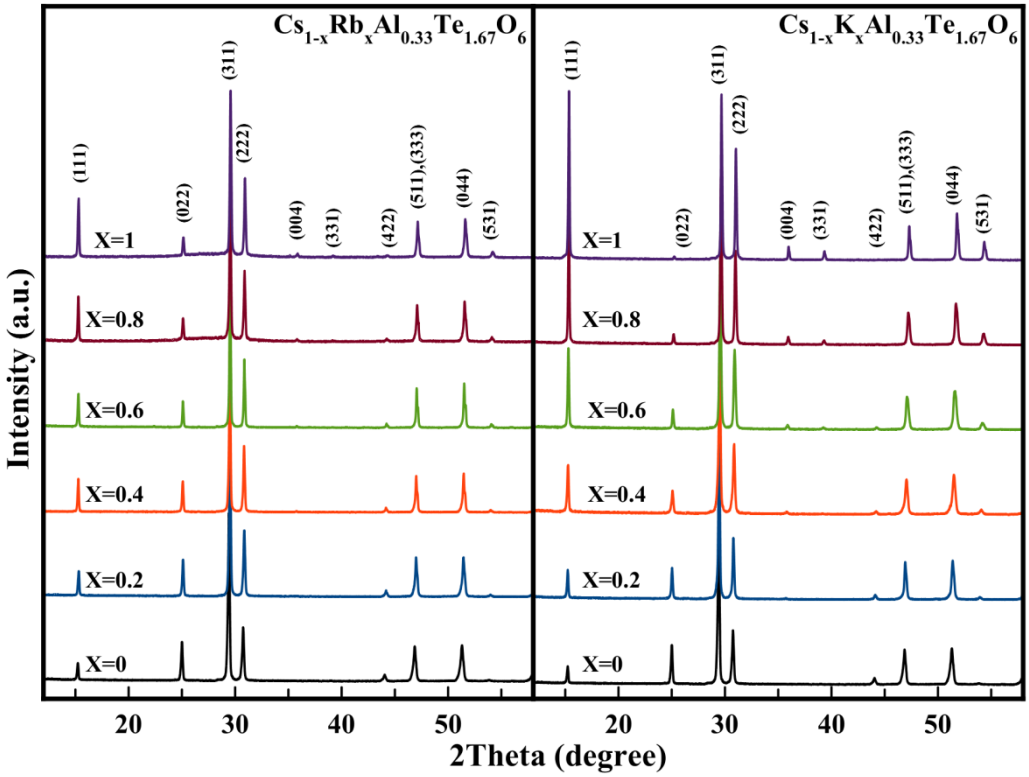

Fig.1 XRD patterns of $Cs_{1-x}Rb_xAl_{0.33}Te_{1.67}O_6$and $Cs_{1-x}K_xAl_{0.33}Te_{1.67}O_6$

Fig. 2 shows $A_2B_2O_7$ pyrochlore structure which can be explained based on the interpenetrating networks of B_2O_6 octahedral units and the A_2O' chain. However, the interaction between A and O' is relatively weak and the 'back-bone' of the structure is the B_2O_6 octahedral units. The weak interaction between the B_2O_6 network and A_2O' chain thus allows some

vacancies in the chain leading to several types of defect pyrochlores such as □AB_2O_6□ and $A_2B_2O_{7-x}$□$_x$.

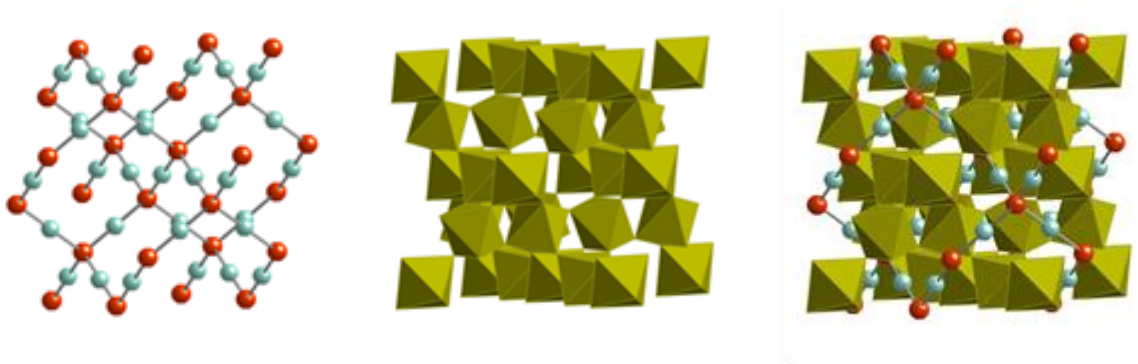

Fig. 2: (a) A_2O' chain [red balls represent O], (b) B_2O_6 octahedral network, (c) $A_2B_2O_7$ pyrochlore structure

In the AB_2O_6 defect cubic pyrochlore or the β-pyrochlore structure, O' and one of A in the A_2O' chain are vacant while the B_2O_6 network remains unchanged. Thus, the structure has many vacancies and there are several possible crystallographic sites for the remaining A cation including the 8b, 16d, and 32e position (Fig. 3). In general, small cation like Na prefers 16d site[18] while K, Rb, and Cs usually occupy 8b or 32e position.[19-20] However, The XRD patterns of our samples suggest no indication of A cations (Cs, Rb, and K) being at other positions other than the normal 8b site but small deviations from this ideal position, like the 32e position, is also possible.

It is worth to note that the displacive disorder of A cation from 8b to 32e position result in a nonlinear increase of cell parameters in $AAl_{0.33}W_{1.67}O_6$; A = Cs, Rb, and K.[21] However, such anomaly is not observed in this work although the samples are quite similar. Plots of calculated cell parameters versus substituting content are linear in both series (Fig. 4). As both K^+ (1.51 Å) and Rb^+ (1.61 Å) are smaller than Cs^+ (1.74 Å), increasing their content results in smaller cell parameters as expected.[22-23] However, the main network of the structure is the B_2O_6 octahedral network, changing A cations has a much smaller effect on the cell parameters comparing to changing the B cations. Similar results were reported by Castro and Rasines.[24]

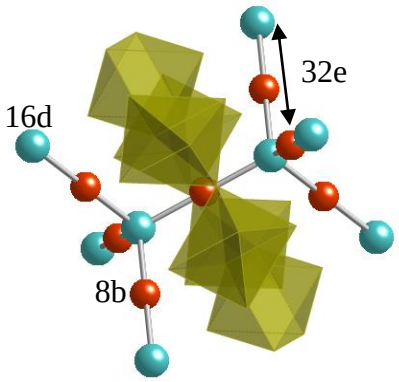

Fig. 3 Crystallographic sites for A cation in AB_2O_6 defect pyrochlore. Ball and stick model shows the arrangement of A_2O' chain and the polyhedral represent B_2O_6 octahedral network.

The linear relationship between the cell parameters and the substituting content also confirms that K, Rb, and Cs randomly distribute in the A position of the structure without changing the main B_2O_6 network. In addition, it is known that K containing defect pyrochlore oxides can sometimes contain water molecules in the structure. In those cases, cell parameters are often deviated from the expected values. Therefore, lack of any deviation from the linear line in Fig. 4 led us to believe that our samples do not contain water molecules.

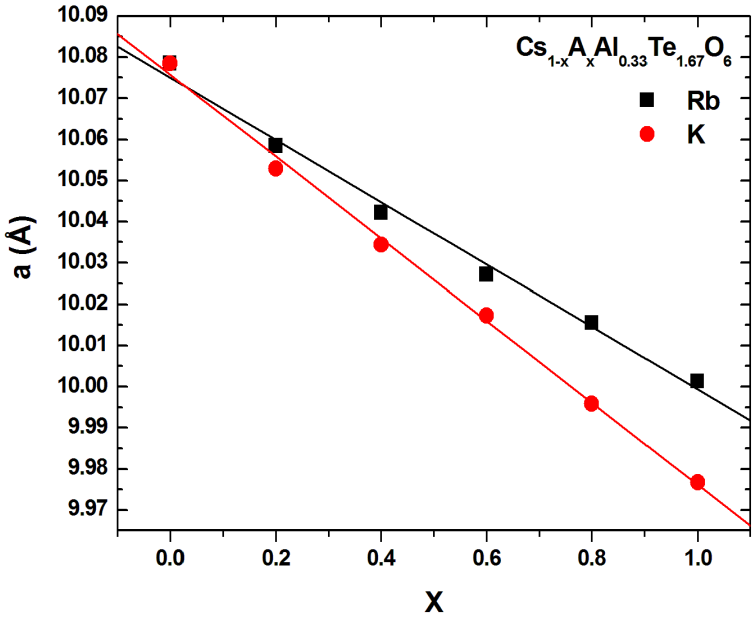

Fig.4 Plots of cell parameters versus Rb and K content

4.2 X-ray photoelectron spectroscopy and calculations

XPS survey spectra of $CsAl_{0.33}Te_{1.67}O_6$ (CATO), $RbAl_{0.33}Te_{1.67}O_6$ (RATO), and $KAl_{0.33}Te_{1.67}O_6$ (KATO) show the corresponding elemental compositions in each compound (Fig. 5). Cs3d, Rb3d and K2p XPS spectra in Fig.6 give semi-quantitative results on the composition of the prepared samples. The obtained binding energies are close to those reported in literature.[25-28] The trend in peak areas of each element in the samples agrees well with their nominal composition.

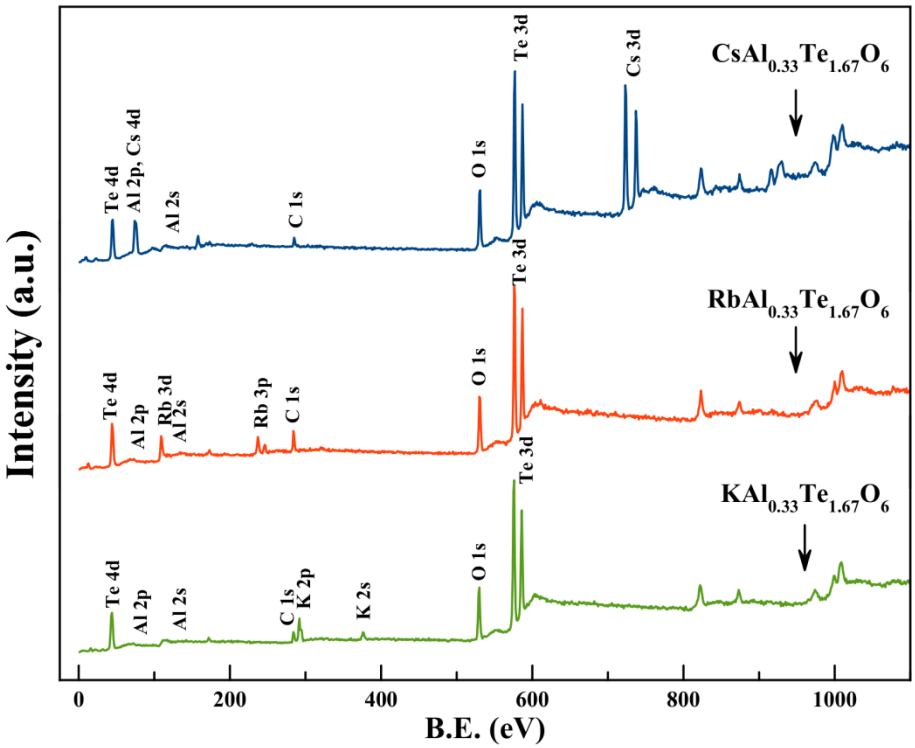

Fig. 5: XPS survey spectra of $CsAl_{0.33}Te_{1.67}O_6$, $RbAl_{0.33}Te_{1.67}O_6$, and $KAl_{0.33}Te_{1.67}O_6$

XPS spectra of $Te3d_{5/2}$ are also examined to probe oxidation states of Te in the samples. As seen in Fig. 7, all spectra show small asymmetry with a tail on the lower energy region. These spectra are fitted using two Gaussian-Lorentzian peaks; one represents Te^{4+}at lower binding energy and the other represents Te^{6+}. For comparison, $Te3d_{5/2}$ spectra of $CsTe_2O_6$ (CTO), a known compound which contains both $Te^{4+}$and Te^{6+}, are also shown and fitted with the same method here. The binding energy and peak area of each peak are

summarized in Table 2. It is interesting to note that while the binding energies of the observed Te^{6+} are close to the reported values, those of Te^{4+} in $Cs_{1-x}A_xAl_{0.33}Te_{1.67}O_6$ (A = K, Rb, and Cs) are slightly smaller than most reported values forTe^{4+}.[29-30] On the other hand, the obtained values are too high to be assigned to Te(0) or Te^{2-} states.[31] As chemical environments affect the binding energy, binding energy of Te^{4+} in these samples which is in the unique compressed octahedra is expected to be different from that of Te^{4+} in TeO_2 standard. In fact, our values are close to that reported in $Gd_2(Ti_{2-y}Te_y)O_7$ pyrochlores.[32]

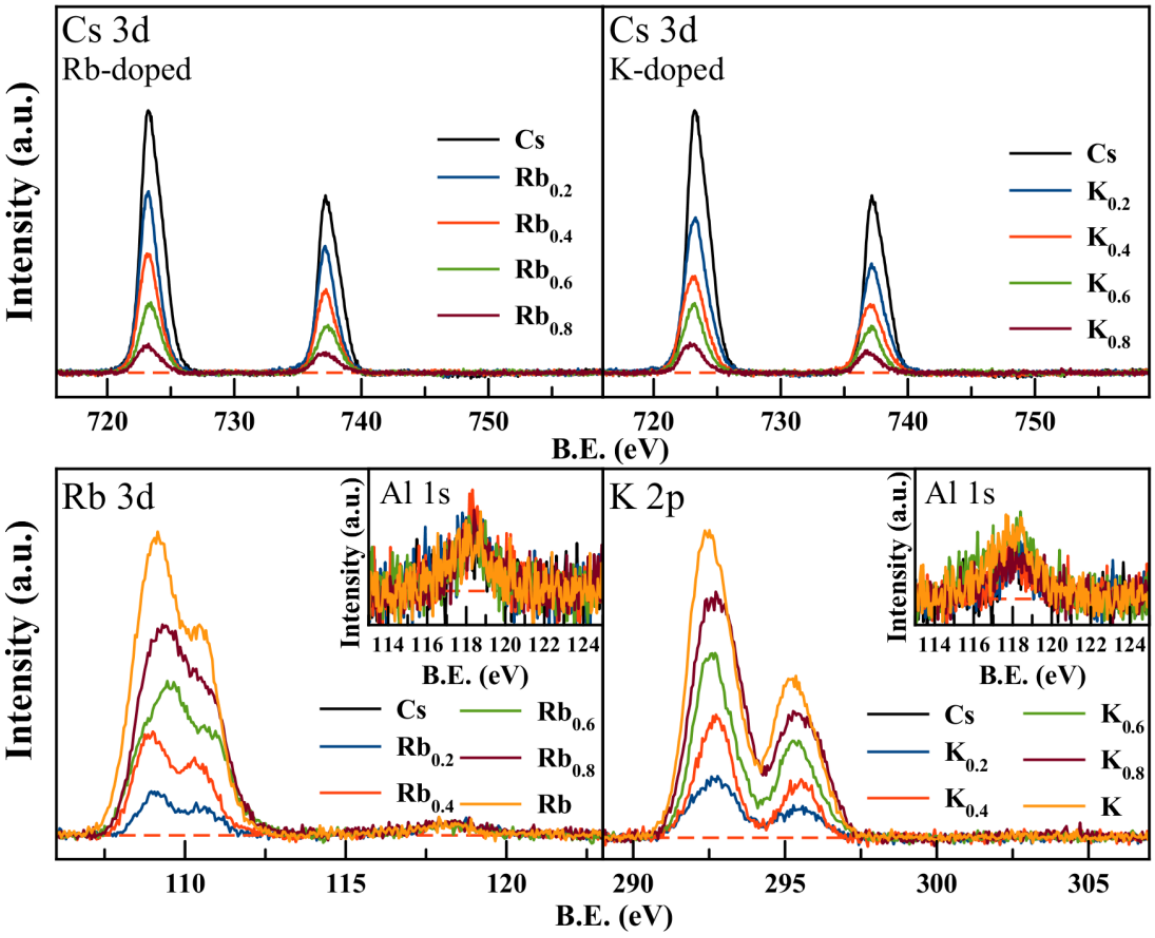

Fig. 6: Cs3d, Rb3d, K2p and Al 1s XPS spectra of $Cs_{1-x}Rb_xAl_{0.33}Te_{1.67}O_6$and $Cs_{1-x}K_xAl_{0.33}Te_{1.67}O_6$

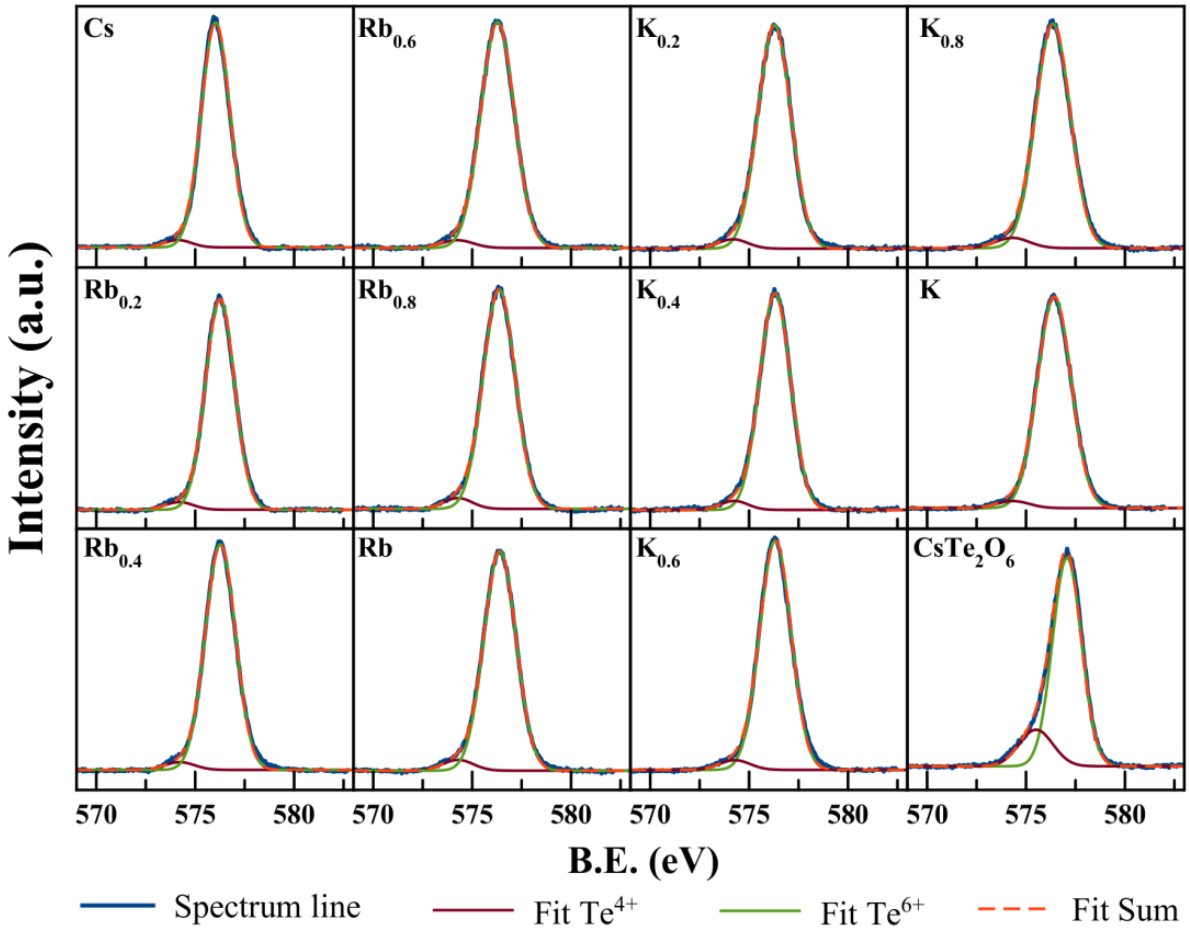

Fig. 7: XPS $Te3d_{5/2}$ spectra of the samples

It is difficult to quantitatively conclude the amount of Te^{4+} in the samples based solely on the peak areas. Nevertheless, the existence of $Te^{4+}$is obvious and its amount in the cubic pyrochlore samples is very low. The presence of small amount of $Te^{4+}$is a result of small deviation in stoichiometry as reported by Li et al.[7] who concluded that the composition of the prepared $CsAl_{0.33}Te_{1.67}O_6$ was actually $CsAl_{0.30}Te_{1.70}O_6$. Small amount of Te^{6+} must then be reduced to Te^{4+} to maintain charge neutrality. Te $3d_{5/2}$ XPS results reported here reveal the existence of Te^{4+} in all samples with similar peak areas suggesting that the Rb and K substituted samples contain similar defects with a similar amount.

Table 1: Te $3d_{5/2}$ fitting results

	Te^{6+}		Te^{4+}			
Comp. (X)	B.E. (eV)	FWHM (eV)	B.E. (eV)	FWHM (eV)	Ratio of Te^{6+}: Te^{4+} (1.67)	R^2
0	576.03	1.70	574.12	1.62	1.62:0.05	0.9983
			Rb-doped			
0.2	576.25	1.72	574.19	1.68	1.61:0.06	0.9991
0.4	576.27	1.79	574.22	1.78	1.62:0.05	0.9987
0.6	576.28	2.00	574.25	1.86	1.62:0.05	0.9994
0.8	576.36	1.90	574.28	1.68	1.60:0.07	0.9992
1.0	576.40	1.85	574.28	1.80	1.60:0.07	0.9995
			K-doped			
0.2	576.28	1.89	574.29	1.68	1.61:0.06	0.9993
0.4	576.32	1.79	574.33	1.72	1.60:0.07	0.9995
0.6	576.32	1.84	574.34	1.61	1.60:0.07	0.9982
0.8	576.35	2.02	574.43	1.99	1.60:0.07	0.9987
1.0	576.42	1.97	574.46	1.87	1.61:0.06	0.9992
			$CsTe_2O_6$			
-	577.07	1.72	575.50	2.00	1.66:0.44 ($Te^{6+}_{1.5}$: $Te^{4+}_{0.5}$)	0.9981

XPS spectra at valence band region (Fig. 8a) give valuable information regarding electronic structure of the samples. Like most oxides, the top of the valence band is predominantly O2p. The outstanding feature of the spectra is the position of alkali p orbitals which is at about 10, 13, and 17 eV for Cs 5p, Rb 4p, and K 3p, respectively. The positions of these states are similar to values in other reports.[28,33-34] Rb 4p and K 3p bands are quite separated from O 2p near the top of the valence band and should not have much contribution in it. Thus, the spectral feature and position of the valence band in Rb and K containing samples are very similar. This also implies that any effects from the difference in bond distances and angles are insignificant. Two samples containing Cs have similar spectra though there are some differences as both samples contain quite a different composition and have related, but different, crystal structure. As Cs5p bands are clearly overlapping with O 2p, Cs is believed to contribute to the valence band. The overlapping between Cs 5p and O 2p in the valence band is observed in many oxides.[35-36] The contribution from Cs5pbroadens the valence band thus causes the shift in its position comparing to the other two samples with no Cs. In addition, the spectral shape of $CsTe_2O_6$ valence band is different from others. Besides the dominant peaks contributed by O 2p, there is another small peak on top of that the valence band maximum (VBM) (Fig. 8b).

To gain deeper understandings, band structure calculation was performed for $CsTe_2O_6$. Valence band of $CsTe_2O_6$ may be divided into three regions (Fig. 8c). The small peaks at VBM consist of O 2p and Te 5s orbitals. The wide region at approximately -1 to -6 eV is predominantly O 2p with a small contribution from Te 4d orbital and the sharp peak at about -6 to -8 eV is formed mainly by Cs 5p orbital with some contribution from Te 5p. These main features of the valence band are qualitatively comparable to the obtain XPS spectra. It is interesting to note that the small peak at VBM is not observed in XPS spectra of the $AAl_{0.33}Te_{1.67}O_6$ series. However, as proposed by Li et al.[7] and deduced from Te $3d_{5/2}$ spectra, $AAl_{0.33}Te_{1.67}O_6$ samples should contain only about 3% of Te^{4+} which is very little comparing to 25% in $CsTe_2O_6$. Besides, it is difficult to compare the spectra of these two series as they have a different structure which leads to the different position of Te 5s.

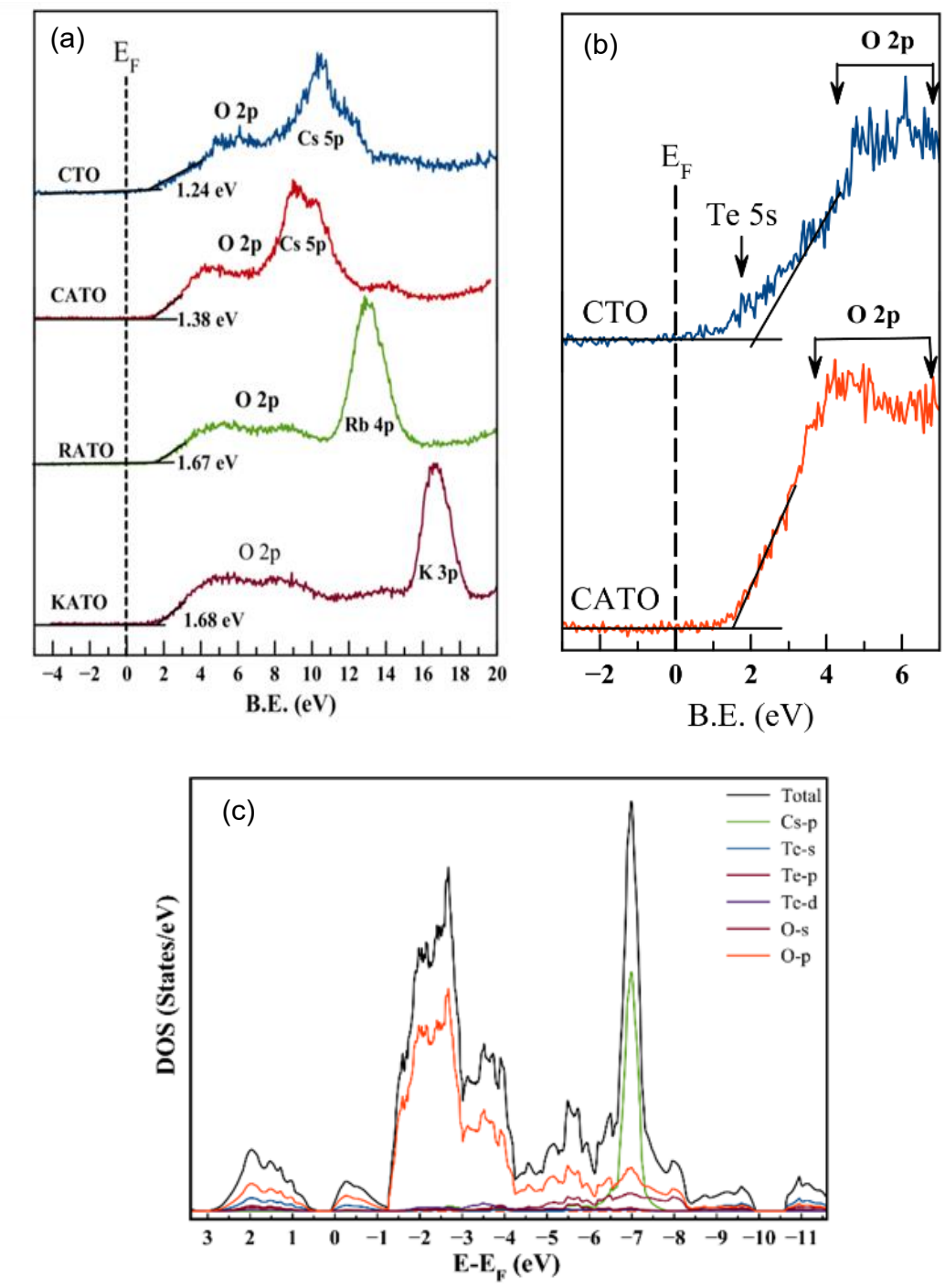

Fig. 8 XPS valence band spectra of $CsTe_2O_6$ and $AAl_{0.33}Te_{1.67}O_6$ (A = Cs, Rb, and K) (a) and the close-up of Cs containing samples showing an additional small peak near the Fermi level (b). (c) shows the calculated valence band of $CsTe_2O_6$

4.3 Electrical conductivity

Electronic conductivity of $Cs_{1-x}A_xAl_{0.33}Te_{1.67}O_6$, A = Rb and K decrease with increasing A content. The effect is very significant as room temperature conductivity of $KAl_{0.33}Te_{1.67}O_6$and $RbAl_{0.33}Te_{1.67}O_6$ are 10^3 and 10^5 times lower than that of $CsAl_{0.33}Te_{1.67}O_6$, respectively (Fig. 9). Electronic conductivity in mixed valence oxides can be usually explained based on two mechanisms, the band conduction and the small polaron hopping. While the temperature dependence conductivity in band conduction can be explained by the Arrhenius' equation: $\sigma = Ae^{(-Ea/kT)}$, that of the polaron hopping is best described by $\sigma T = Be^{(-Eh/kT)}$ where A and B are pre-exponential constant, k is Boltzmann constant, Ea and Eh are activation energy, and T is absolute temperature. Conductivity of all samples are plotted based on both models as shown in Fig. 7a and b and the activation energy are calculated and summarized in Table 2. The activation energy of conduction calculated from both models follow the same trend. The lower Cs content, the higher the activation energy. As the linear relationship is observed in both cases with similar R^2, it is difficult to conclude the conduction mechanism of the samples with the present results. However, conductivity and activation energy of small polaron hopping usually relate to the hopping distance. The longer M-O bond distance should result in the higher activation energy and lower conductivity.[37-38] As XPS results suggest no significant difference in defect concentration of the samples, the change in hopping conductivity should depend on the carrier mobility which directly relates to the hopping distance. It is improbable that the difference in the hopping distances, M-O, in our samples is large enough to result in such a large difference in the conductivity. Thus, we believed that band conduction is dominant in this temperature range. Interestingly, Siritanon et. al.[6] previously reported that the Arrhenius plot of $Cs(M,Te)_2O_6$ are not linear in temperature range 50-300K and concluded that the samples exhibit variable range hopping conduction as the plots of log conductivity vs. $1/T^{1/4}$ are linear. Therefore, the samples have different conduction processes at different temperatures. In fact, crossover from variable range hopping conduction to thermally activated band conduction from low to high temperatures have been reported in many systems and believed to also be the case here.[39-40]

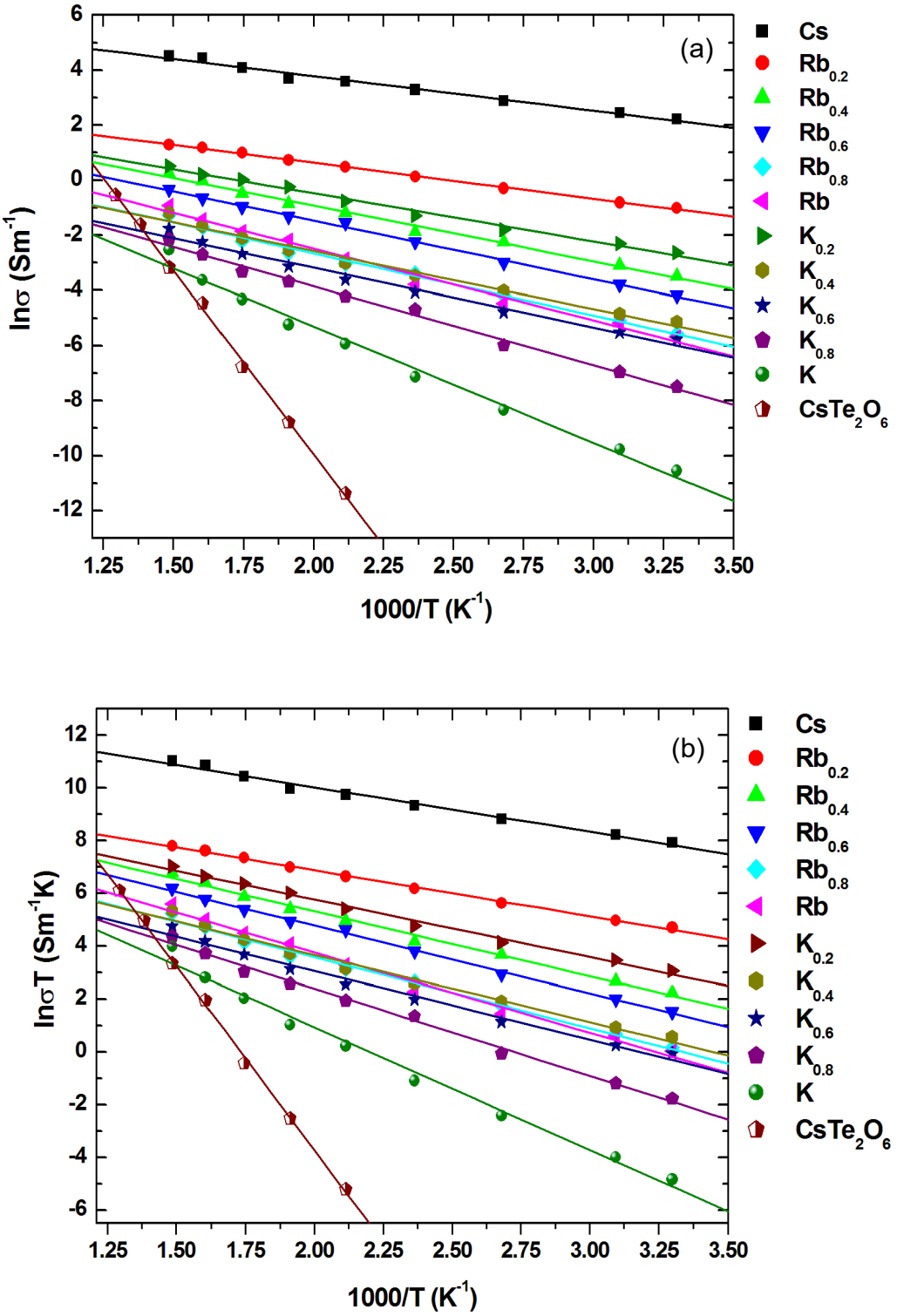

Fig. 9 Electronic conductivity of $Cs_{1-x}A_xAl_{0.33}Te_{1.67}O_6$ (A = Rb and K) and $CsTe_2O_6$ samples fitted with (a) Arrhenius equation and (b) polaron hopping model

Table 3: Activation energy and R^2 obtained from fitting the electronic conductivity of $Cs_{1-x}A_xAl_{0.33}Te_{1.67}O_6$; A = Rb and K samples with band conduction and small polaron hopping.

X.	Band conduction		Small polaron hopping	
	E_a (eV)	R^2	E_h (eV)	R^2
0	0.108	0.9854	0.146	0.9875
Rb-doped				
0.2	0.113	0.9985	0.150	0.9976
0.4	0.174	0.9921	0.212	0.9922
0.6	0.183	0.9972	0.220	0.9977
0.8	0.194	0.9919	0.231	0.9926
1.0	0.224	0.9870	0.261	0.9877
K-doped				
0.2	0.151	0.9914	0.188	0.9916
0.4	0.180	0.9856	0.218	0.9863
0.6	0.186	0.9855	0.224	0.9862
0.8	0.247	0.9934	0.285	0.9940
1.0	0.364	0.9888	0.402	0.9890
$CsTe_2O_6$				
-	1.15	0.9987	1.20	0.9988

4.4 Optical property

The UV-Vis absorption spectra of $CsTe_2O_6$ and $AAl_{0.33}Te_{1.67}O_6$, A = Cs, Rb, and K is shown in Fig. 10a and the band gap energy obtained from the extrapolations (Fig. 10b) are summarized in Fig. 12. Although most oxides containing Cs and Te have large band gap and white color, the band gap of $CsTe_2O_6$ is only about 1.4 eV and the compound is dark brown. The unusually small band gap is a result of Te^{4+}, Te^{6+} intervalence charge transfer (IVCT) which gives rise to the absorption in a visible region corresponding to the transition from $Te^{4+}5s^2$ to $Te^{6+}5s^0$. Although there are very few reports on Te^{4+}/Te^{6+} charge transfer, similar mechanism is widely studied in other mixed valence systems including those with post transition cations like Sb, Sn, Tl.[41-42]

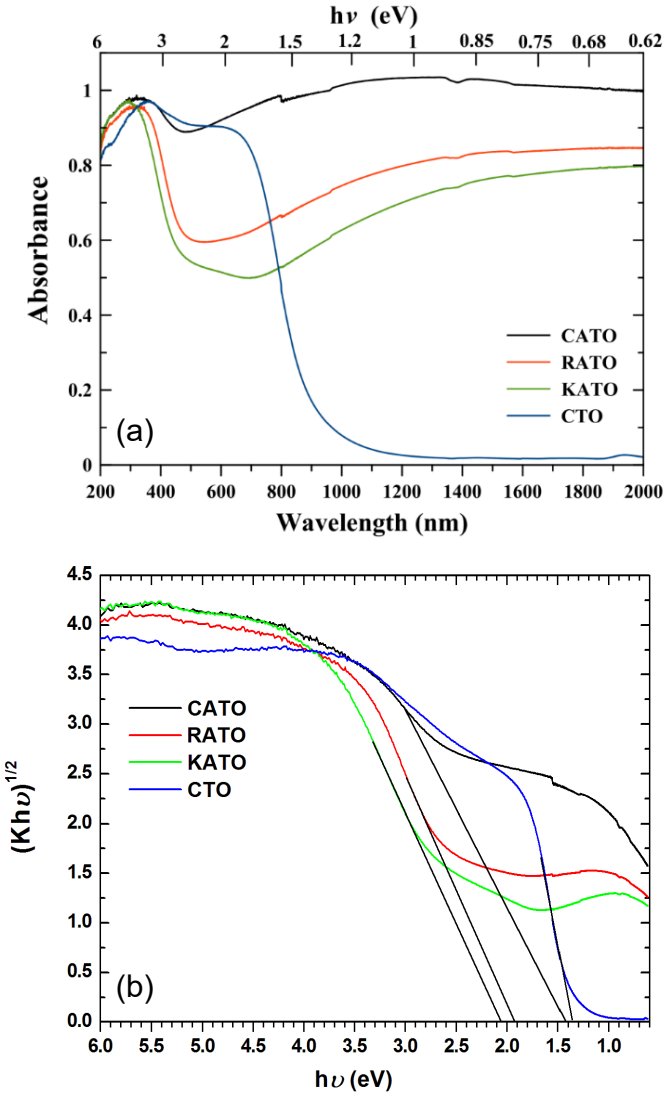

Fig. 10: UV-Vis spectra (a) and extrapolation of the band gap energy (b) of $CsTe_2O_6$ and $AAl_{0.33}Te_{1.67}O_6$ (A = Cs, Rb, and K)

UV-Vis spectra of$AAl_{0.33}Te_{1.67}O_6$series are obviously different from that of $CsTe_2O_6$ although the compounds also containTe^{4+}/Te^{6+} mixed valency. However, Te^{4+} and Te^{6+} in $CsTe_2O_6$ are in different crystallographic sites while those in $AAl_{0.33}Te_{1.67}O_6$ are in the same one. As λ_{max} of absorption should be directly related to the energy difference between Te^{4+} $5s^2$and Te^{6+} $5s^0$, the more similarity of the environment around Te^{4+} and Te^{6+} in $AAl_{0.33}Te_{1.67}O_6$ results in absorptions at a longer wavelength. Therefore, it is concluded here that the very broad and strong absorption centering at long wavelengths is associated with IVCT of Te^{4+} and Te^{6+}. Mizoguchi et al.[41] also reported similar diffuse reflectance spectra of $BaSn_{1-x}Sb_xO_3$ which contain mixed valence ions and show a very broad absorption band due to IVCT.

4.5 Discussions

It has been established that $CsAl_{0.33}Te_{1.67}O_6$ shows relatively high conductivity.[6] Li et. al.[7] concluded that the conductivity comes from small deviations from stoichiometry which results in small amount of Te^{4+} producing mixed valence compounds. The n-type behavior in these series of compounds is explained by the presence of donor defect levels originating from Te^{4+}. In general, type of M cations in $Cs(M,Te)_2O_6$ affects the conductivity of the compounds as small M cation reduces M/Te-O distance thus destabilizes Te^{4+} in the structure increasing their energy level. In addition, some M cations could provide orbitals with appropriate energy to overlap with Te 5s which increase the conductivity.

When Cs is replaced by Rb and K in $Cs_{1-x}A_xAl_{0.33}Te_{1.67}O_6$, the difference in conductivity is very pronounced although the same Al is present. Additionally, samples containing Rb and K have much less conductivity despite the smaller cell parameters. XPS results obtained in this work do not indicate any difference in the number of Te^{4+}, hence the number of defect levels, in all samples. In addition, we have also prepared and measured conductivity of $CsAl_xTe_{2-x}O_6$ and $RbAl_xTe_{2-x}O_6$ with different x values. As shown in Fig. 11, the conductivity of both series exhibit similar Al content dependency which is also in agreement with the previous work.[7] It is, therefore, reasonable to conclude that the type and the amount of defect, e.g. Te^{4+}, are similar in all samples. If the number of Te^{4+} is similar, then the difference in conductivity must be related toTe^{4+} energy level relative to the conduction band.

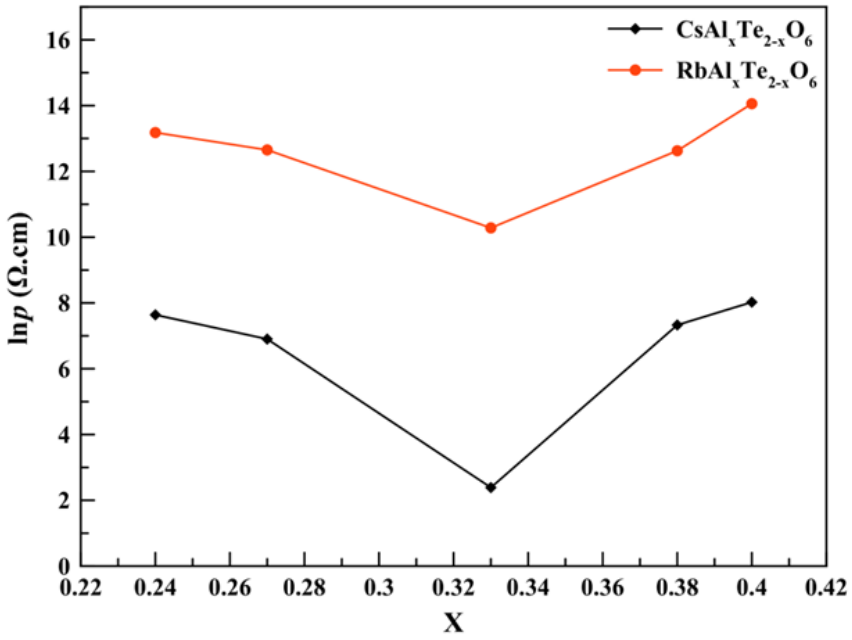

Fig. 11 Resistivity of the $AAl_xTe_{2-x}O_6$ (A = Cs and Rb)**.** Note that resistivity of $KAl_xTe_{2-x}O_6$ samples when x is not equal to 0.33 are too high to be measured with the current technique

Based on the band gap energy obtained from UV-Vis results and the VBM position obtained from XPS valence band spectra, we propose schematic band structure diagram of the samples as depicted in Fig.12. From the figure, the difference between Fermi energy level and the bottom of the conduction band (E_d) is obtained. Generally, the band diagrams of these four samples represent their semiconducting behavior. However, the activation energies of conduction indicate that their behavior are different. The activation energy of conduction of $CsTe_2O_6$ (1.15 eV) (Fig.9) is in the same order with its band gap energy suggesting the intrinsic semiconducting behavior. The conductivity of this sample is small because large energy is required to activate electrons across the band gap. It is noteworthy that E_d and the activation energy of conduction in $CsTe_2O_6$ are significantly different which indicates that there is no defect level at the Fermi energy level (E_F). On the other hand, the activation energies of $AAl_{0.33}Te_{1.67}O_6$ are close to E_d and much smaller than their band gap energy which suggests the presence of defect levels close to the conduction band within the band gap. The presence of such defect levels is a characteristic of n-type semiconductors which agrees well with the

negative Seebeck coefficients.[6] E_d in these three samples indicate the position of defect levels relative to conduction band minimum (CBM) which determines conductivity of the samples.

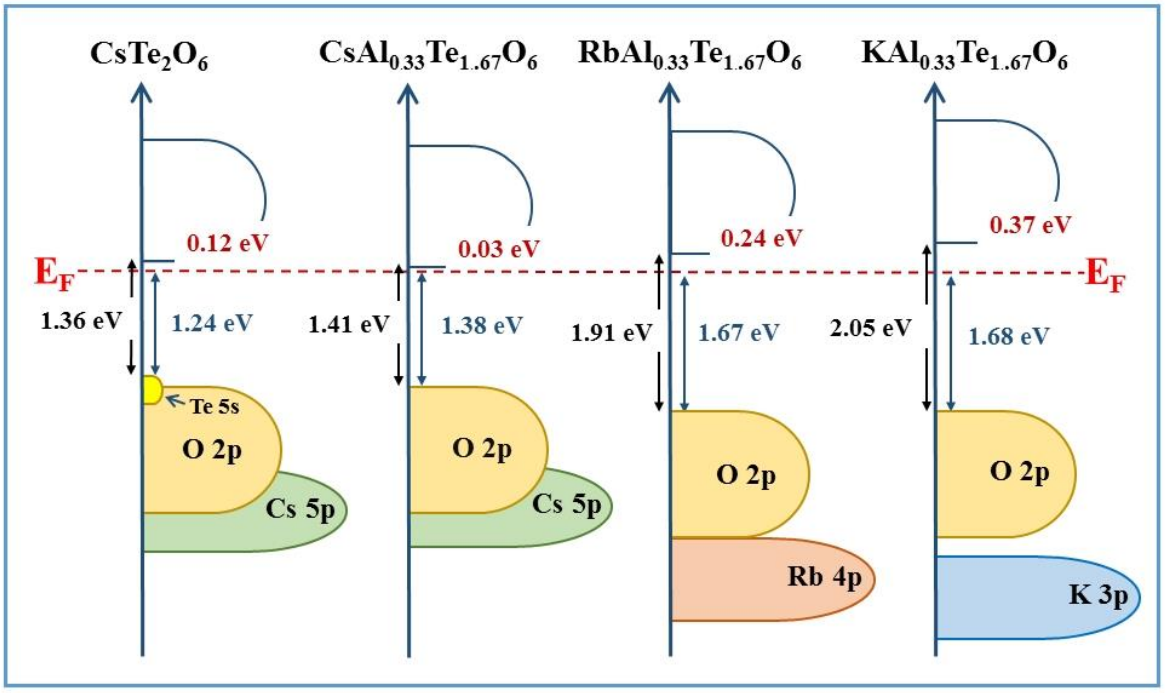

Compounds	Valence band position (eV)	Band gap energy (eV)	E_d (eV)	Activation energy of conduction (eV)
$CsTe_2O_6$	1.24	1.36	0.12	1.15
$CsAl_{0.33}Te_{1.67}O_6$	1.38	1.41	0.03	0.108
$RbAl_{0.33}Te_{1.67}O_6$	1.67	1.91	0.24	0.224
$KAl_{0.33}Te_{1.67}O_6$	1.68	2.05	0.37	0.364

Fig. 12 Schematic band structure of $CsTe_2O_6$ and $AAl_{0.33}Te_{1.67}O_6$ (A = Cs, Rb, and K)

Replacing Cs with Rb and K have two effects on the band diagram; lowering the VBM and increasing the band gap energy. It should be noted that lowering VBM in these cases is not the only cause of increasing the band gap. Without the presence of Cs, VBM of both RATO and KATO is about 0.3 eV lower in energy. However, the band gap differences between the samples are 0.5-0.6 eV. As the conduction band should be mainly Te 5s with some contribution

from Al and O, Te/Al-O bond distance and Te/Al-O-Te/Al bond angle must play important roles in determining the CBM. Additional detail studies are required to further explain this matter. Nevertheless, the combination of VBM lowering and band gap energy increasing when Cs is replaced with Rb and K result in larger E_d and consequently lower conductivity.

5. Conclusion

Complete solid solutions of general formula $Cs_{1-x}A_xAl_{0.33}Te_{1.67}O_6$; A = Rb and K with x =0, 0.2, 0.4, 0.6, 0.8, and 1 have been successfully prepared by solid state reaction. The compounds adopt AB_2O_6 defect pyrochlore structure with Cs, Rb, and K in A site. Cell parameters of the solid solutions vary linearly with the substituting content. Detail studies by XPS technique indicate that all samples contain similar amount of Te^{4+}/Te^{6+} mixed valency. Such mixed valency is the origin of electrical conductivity in these compounds which behave like n-type semiconductors. It is also the origin of absorption at long wavelengths which results in unusually dark colors. The results obtained from XPS and UV-Vis absorption allow us to propose the schematic band structure of the compounds which could explain both the electrical and optical properties of the compounds. In general, the valence band is composed of mainly O 2p orbital while the conduction band is predominantly Te 5s. Because of small deviation from stoichiometry, small number of Te^{6+} is reduced to Te^{4+} in the structure introducing the donor defect levels close to the CBM. Excitation of electrons from such levels to the conduction band leads to electrical conductivity. Thus, the difference between these defect levels and the conduction band (E_d) determines the activation energy of conduction and, consequently, the conductivity of the compounds. Among all samples studied in this work, $CsAl_{0.33}Te_{1.67}O_6$ shows the highest conductivity. Replacing Cs with Rb or K lowers the VBM and increases the band gap energy which result in a larger E_d, thus the lower conductivity.

6. References

[1] Sleight, A.W.; Gilson, J. L.; Bierstedt, P.E., High-temperature superconductivity in the $BaPb_{1-x}Bi_xO_3$ systems. *Solid State Commun.* **1975**, 17, 27-28.

[2] Cava, R.J.; Batlogg, B.; Ramirez, G. P.; Krajewski, J. J.; Peck Jr. W. F.; Rupp Jr. L. W.; Cooper A. S., Superconductivity at 3.5 K in $BaPb_{0.75}Sb_{0.25}O_3$: why is Tc so low? *Nature*. **1989**, 339, 291-293.

[3] Noguchi, S.; Sakata, H., Electrical properties of undoped In_2O_3 films prepared by reactive evaporation. *J. Phys. D: Appl. Phys.* **1980**, *13*, 1129

[4] Cai, S.; Li, Y.; Chen, X.; Ma, Y.; Liu, X.; He, Y., Optical and electrical properties of Ta-doped ZnSnO3 transparent conducting films by sol–gel. *J. Mater. Sci: Mater. Electron.* **2016**, *27*, 6166-6174.

[5] O'Neil, D. H.; Kuznetsov, V. L.; Jacobs, R. M.; Jones, M. O.; Edwards, P. P., Structural, optical and electrical properties of $In_4Sn_3O_{12}$ films prepared by pulsed laser deposition. *Mater. Chem. Phys.* **2010**, *123*, 152-159.

[6] Siritanon, T.; Laurita, G.; Macaluso, R. T.; Millican, J. N.; Sleight, A. W.; Subramanian, M., First observation of electronic conductivity in mixed-valence tellurium oxides. *Chem. Mater.* **2009**, *21*, 5572-5574.

[7] Li, J.; Siritanon, T.; Stalick, J. K.; Sleight, A. W.; Subramanian, M., Structural studies and electrical properties of Cs/Al/Te/O phases with the pyrochlore structure. *Inorg. Chem.* **2011**, *50*, 5747-5754.

[8] Howng, W.-Y.; Thorn, R., Investigation of the electronic structure of $La_{1-x}(M^{2+})_xCrO_3$, Cr_2O_3 and La_2O_3 by X-ray photoelectron spectroscopy. *J. Phys. Chem. Solids.* **1980,** *41*, 75-81.

[9] Lv, Y.; Yao, W.; Zong, R.; Zhu, Y., Fabrication of Wide–Range–Visible Photocatalyst Bi_2WO_{6-x} nanoplates via Surface Oxygen Vacancies. *Sci. Rep.* **2016***, 6,* 19347*.*

[10] Guje, R.; Ravi, G.; Palla, S.; Rao, K. N.; Vithal, M., Synthesis, characterization, photocatalytic and conductivity studies of defect pyrochlore $KM_{0.33}Te_{1.67}O_6$ (M= Al, Cr and Fe). *Mater. Sci. Eng. B* **2015**, *198*, 1-9.

[11] Morales, A. E.; Mora, E. S.; Pal, U., Use of diffuse reflectance spectroscopy for optical characterization of un-supported nanostructures. *Rev. Mex. Fis. S* **2007**, *53*, 18.

[12] Kresse, G.; Hafner, J., Ab initiomolecular dynamics for open-shell transition metals. *Phys. Rev. B* **1993**, *48*, 13115-13118.

[13] Fuchs, F.; Furthmüller, J.; Bechstedt, F.; Shishkin, M.; Kresse, G., Quasiparticle band structure based on a generalized Kohn-Sham scheme. *Phys. Rev. B* **2007**, *76*, 115109.

[14] Perdew, J. P.; Burke, K.; Ernzerhof, M., Generalized Gradient Approximation Made Simple. *Phys. Rev. Lett.* **1996**, *77*, 3865-3868.

[15] Blöchl, P. E., Projector augmented-wave method. *Phys. Rev. B* **1994**, *50*, 17953-17979.

[16] Kresse, G.; Joubert, D., From ultrasoft pseudopotentials to the projector augmented-wave method. *Phys. Rev. B* **1999,** *59*, 1758-1775.

[17] Subramanian, M.; Aravamudan, G.; Rao, G. S., Oxide pyrochlores-a review. *Prog. Solid State Chem.* **1983**, *15*, 55-143.

[18] Murphy, D. W.; Dye, J. L.; Zahurak, S. M., Alkali metal insertion in the pyrochlore structure. *Inorg. Chem.*, **1983**, 22, 3679-3681**.**

[19] Barnes, P. W.; Woodward, P. M.; Lee, Y.; Vogt, T.; Hriljac, J. A.; Pressure-Induced Cation Migration and Volume Expansion in the Defect Pyrochlores $ANbWO_6$ (A = NH_4^+, Rb^+, H^+, K^+) *J. Am. Chem. Soc.,* **2003**, 125, 4572-4579.

[20] Whittle, K. R.; Lumpkin, G. R.; Ashbrook, S. E.; Neutron diffraction and MAS NMR of Cesium Tungstate defect pyrochlores. *J. Solid State Chem.,* **2006**, 179, 512-521.

[21] Thorogood, G. J.; Kennedy, B. J.; Peterson, V. K.; Elcombe, M. M.; Kearley, G. J.; Hanna, J. V.; Luca, V., Anomalous lattice parameter increase in alkali earth aluminium substituted tungsten defect pyrochlores. *J. Solid State Chem.* **2009**, *182*, 457-464.

[22] Shannon, R. T.; Prewitt, C. T., Effective ionic radii in oxides and fluorides. *Acta Crystallogr. B* **1969**, *25*, 925-946.

[23] Shannon, R. t., Revised effective ionic radii and systematic studies of interatomic distances in halides and chalcogenides. *Acta Crystallogr. A* **1976**, *32*, 751-767.

[24] Castro, A.; Rasines, I.; Turrillas, X., Synthesis, X-ray diffraction study, and ionic conductivity of new AB_2O_6 pyrochlores. *J. Solid State Chem.* **1989**, *80*, 227-234.

[25] Marschall, R.; Mukherji, A.; Tanksale, A.; Sun, C.; Smith, S. C.; Wang, L.; Lu, G. Q. M., Preparation of new sulfur-doped and sulfur/nitrogen co-doped $CsTaWO_6$ photocatalysts for hydrogen production from water under visible light. *J. Mater. Chem.* **2011**, *21*, 8871-8879.

[26] Guo, C.; Yin, S.; Dong, Q.; Sato, T., Near-infrared absorption properties of Rb_xWO_3 nanoparticles. *CrystEngComm* **2012**, *14*, 7727-7732.

[27] Ravi, G.; Veldurthi, N. K.; Palla, S.; Velchuri, R.; Pola, S.; Reddy, J. R.; Vithal, M., Synthesis, characterization and photocatalytic activity of $KAl_{0.33}W_{1.67}O_6$ and $Sn_{0.5}Al_{0.33}W_{1.67}O_6\,xH_2O$. *Photochem. Photobiol.* **2013**, *89*, 824-831.

[28] Atuchin, V.; Kesler, V.; Meng, G.; Lin, Z., The electronic structure of $RbTiOPO_4$ and the effects of the A-site cation substitution in $KTiOPO_4$-family crystals. *J. Phys. Condens. Matter.* **2012**, *24*, 405503.

[29] Sathiya, M.; Ramesha, K.; Rousse, G.; Foix, D.; Gonbeau, D.; Guruprakash, K.; Prakash, A.; Doublet, M.; Tarascon, J.-M., Li_4NiTeO_6 as a positive electrode for Li-ion batteries. *Chem. Commun.* **2013**, *49*, 11376-11378.

[30] Tan, G.; Zhang, X.; Chen, Z., Colossal magnetoresistance effect of electron-doped manganese oxide thin film $La_{1-x}Te_xMnO_3$ (x= 0.1, 0.15). *J. Appl. Phys.* **2004**, *95*, 6322-6324.

[31] Sartz Jr, W. E.; Wynne, K. J.; Hercules, D. M., X-ray photoelectron spectroscopic investigation of Group VIA elements. *Anal. Chem.* **1971**, *43*, 1884-1887.

[32] Heredia, A.; García, M. Q.; Mazariego, J. P.; Escamilla, R., X-ray diffraction and Raman spectroscopy on $Gd_2(Ti_{2-y}Te_y)O_7$ prepared at high pressure and high temperature. *J. Alloy Compd.* **2010**, *504*, 446-451.

[33] Slobodin, B.; Surat, L.; Zubkov, V.; Tyutyunnik, A.; Berger, I.; Kuznetsov, M.; Perelyaeva, L.; Shein, I.; Ivanovskii, A.; Shulgin, B., Structural, luminescence, and electronic properties of the alkaline metal-strontium cyclotetravanadates $M_2Sr(VO_3)_4$,(M= Na, K, Rb, Cs). *Phys. Rev. B* **2005**, *72*, 155205.

[34] Van den Berghe, S.; Laval, J.-P.; Gaudreau, B.; Terryn, H.; Verwerft, M., XPS investigations on cesium uranates: mixed valency behaviour of uranium. *J. nucl. mater.* **2000**, *277*, 28-36.

[35] Waghmode, S. B.; Vetrivel, R.; Hegde, S. G.; Gopinath, C. S.; Sivasanker, S., Physicochemical investigations of the basicity of the cation exchanged ETS-10 molecular sieves. *J. Phys. Chem. B* **2003**, *107*, 8517-8523.

[36] Yang, Y.; Su, X.; Pan, S.; Zhang, M.; Wang, Y.; Han, J.; Yang, Z., Crystal growth and calculation of the electronic band structure and density of states of $Li_3Cs_2B_5O_{10}$. *CrystEngComm* **2014**, *16*, 1978-1984.

[37] Ohtaki, M.; Koga, H.; Tokunaga, T.; Eguchi, K.; Arai, H., Electrical Transport Properties and High-Temperature Thermoelectric Performance of $(Ca_{0.9}M_{0.1})MnO_3$ (M= Y, La, Ce, Sm, In, Sn, Sb, Pb, Bi). *J. Solid State Chem.* **1995**, *120*, 105-111.

[38] Taguchi, H.; Hirata, K.; Kido, H.; Takeda, Y.; Kato, M.; Hirota, K., Hopping conductivity of distorted K_2NiF_4-type $(Ca_{1+x}Nd_{1-x})CrO_4$. *Solid State Sci.* **2009**, *11*, 1222-1225.

[39] Han, M.; Jiang, K.; Zhang, J.; Yu, W.; Li, Y.; Hu, Z.; Chu, J., Structural, electronic band transition and optoelectronic properties of delafossite $CuGa_{1-x}Cr_xO_2$ ($0 \leq x \leq 1$) solid solution films grown by the sol–gel method. *J. Mater. Chem.* **2012**, *22*, 18463-18470.

[40] Okutan, M.; Bakan, H. I.; Korkmaz, K.; Yakuphanoglu, F., Variable range hopping conduction and microstructure properties of semiconducting Co-doped TiO_2. *Phys. B Condens. Matter* **2005**, *355*, 176-181.

[41] Mizoguchi, H.; Chen, P.; Boolchand, P.; Ksenofontov, V.; Felser, C.; Barnes, P. W.; Woodward, P. M., Electrical and optical properties of Sb-doped $BaSnO_3$. *Chem. Mater.* **2013**, *25*, 3858-3866.

[42] Atkinson, L.; Day, P., Charge transfer in mixed-valence solids. Part IV. Electronic spectra of hexachloroantimonates (III, V). *J. Chem. Soc. A* **1969**, 2423-2431.

7. Suggestions for future research

Although not widely studied, the current work has shown that Te-containing oxides could be interesting candidates for many applications as they show n-type semiconducting behavior. In addition, the origin of conduction is now realized through XPS studies. As the conductivity is originated from Te^{4+}/Te^{6+} mixed valency, the electronic conductivity could be manipulated by changing the chemical composition of the compounds. Increasing the conductivity of the compounds in this series is challenging but could result in a completely new group of metallic or superconducting oxides. In addition, the current research also indicates that optical properties of the compounds could be manipulated by changing the elemental composition which is crucial in some applications such as photocatalysis and transparent conducting materials. In fact, it is known that oxides containing cations with diffused s orbital including Te are often good candidates for both photocatalysis and transparent conducting materials.

The compounds in this group have only been synthesized for the first time recently. Some of their interesting properties have been investigated, several more are awaiting to be explored.

Output จากโครงการวิจัยที่ได้รับทุนจาก สกว.

1. ผลงานตีพิมพ์ในวารสารวิชาการนานาชาติ

Anurak Waehayee, Tanachat Eknapakul,Narong Chanlek,Thanundon Kongnok, Surachet Rattanasuporn, Hideki Nakajima, Sirichok Jungthawan, Worawat Meevasana, Theeranun Siritanon, Electrical properties of $AAl_{0.33}Te_{1.67}O_6$ (A = K, Rb, and Cs) mixed valence pyrochlores, (submitted)

**manuscript แนบในภาคผนวก

2. การนำผลงานวิจัยไปใช้ประโยชน์

- เชิงพาณิชย์

ไม่มี

- เชิงนโยบาย

ไม่มี

- เชิงสาธารณะ

ไม่มี

- เชิงวิชาการ

สร้างบัณฑิตใหม่ระดับปริญญาเอก คือ นายอนุรักษ์ แวหะยี

3. อื่นๆ (เช่น ผลงานตีพิมพ์ในวารสารวิชาการในประเทศ การเสนอผลงานในที่ประชุม)

นำเสนอผลงานในงานประชุม Solid State Chemistry 2016, 18^{th} – 23^{rd} September 2016, Prague, Czech Republic (Oral presentation)

ภาคผนวก

Electrical properties of $AAl_{0.33}Te_{1.67}O_6$ (A = K, Rb, and Cs) mixed valence pyrochlores

Anurak Waehayee[a], Tanachat Eknapakul[b],Narong Chanlek[c],Thanundon Kongnok[b], Surachet Rattanasuporn[c], Hideki Nakajima[c], Worawat Meevasana[b,d,e], Theeranun Siritanon[a,d,e]*

[a]School of Chemistry, Institute of Science, 111 University Avenue, Muang,Suranaree University of Technology 30000, Thailand

[b]School of Physics, Institute of Science, Suranaree University of Technology 30000, Thailand

[c]Synchrotron Light Research Institute, Nakhon Ratchasima 30000, Thailand

[d]NANOTEC-SUT Center of Excellence on Advanced Functional Nanomaterials, Suranaree University of Technology, Nakhon Ratchasima 30000, Thailand

[e]Center of Excellence-Advanced Functional Materials, Suranaree University of Technology

Abstracts

The preparation and electronic properties of $Cs_{1-x}A_xAl_{0.33}Te_{1.67}O_6$ (A = K, Rb, and Cs) are reported. Replacing Cs with smaller Rb and K reduces cell parameters of the compounds but does not affect the overall structure. Electronic conductivity of all samples were measured and explained based on the band conduction model. Although XPS $Te3d_{5/2}$ spectra indicate that all samples contain similar amount of Te^{4+}/Te^{6+} mixed valency, their conductivity is varied from about 0.1 S·cm in $CsAl_{0.33}Te_{1.67}O_6$ to 3 x 10^{-5}Scm in $RbAl_{0.33}Te_{1.67}O_6$ and 3 x 10^{-7}S·cm in $KAl_{0.33}Te_{1.67}O_6$ at 300 K. To explain such large differences, the band structure diagrams are proposed based on the UV-Vis spectra and XPS spectra at valence band region. When the obtained activation energy of conduction and the proposed band diagram are considered, it is concluded that $AAl_{0.33}Te_{1.67}O_6$ (A = K, Rb, and Cs) are n-type semiconductors. The defect levels in these samples originate from Te^{4+} whose energy level relative to the conduction band minimum is different from samples to samples. Such differences are affected by Cs content in the structure as Cs seems to lower the band gap energy and increase the valence band maximum. It is the position of these defect levels that determines the electronic conductivity of the compounds.

Introduction

Post transition elements form oxides with interesting structures and properties. Several oxides containing heavy post transition elements are known to have good electronic conductivity due to the presence of diffused s orbitals which results in wide conduction bands and low carrier mobility.[1] Some well-known examples include In_2O_3, $ZnSnO_3$, and $In_4Sn_3O_{12}$.[2-4] However, conducting tellurium oxides are very rare. To our knowledge, the only clear examples are series of defect pyrochlores with general formula $Cs(M,Te)_2O_6$; M = 2+, 3+ and 4+ cations which show n-type semiconducting behavior due to Te^{4+}/Te^{6+} mixed valency.[5]

It has been established that M cations in the mentioned formula play some roles in determining electronic conductivity of the compounds. Smaller M cations reduce the cell parameter which compresses Te^{4+} in the structure and consequently destabilizes it. In addition, suitable M cations could provide orbitals with appropriate energy to overlap with Te 5s which could give rise to samples with higher conductivity. Only one compound in the series, $Cs(Al,Te)_2O_6$, was extensively investigated through detailed structural studies where it was concluded that Te^{4+}/Te^{6+} mixed valency in the compounds is a result of small deviations from stoichiometry.[6] However, the role of Cs in the structure remains unclear. Thus, the objectives of this work are to deepen the understanding of these series of oxides and to study the effects of cations at Cs position on the electronic properties of compounds in $Cs_{1-x}A_xAl_{0.33}Te_{1.67}O_6$; A = Rb and K series.

Experimental Section

All samples were prepared by solid state reaction. The reactants were $CsNO_3$(Sigma-Aldrich, 99+%), $RbNO_3$ (Acros organic, 99.8%), Al_2O_3 (Acros organic, 99+ %, for Rb-doped series), $Al(OH)_3$ (Acros organic, 99.9%, for K-doped series) and TeO_2 (Acros organic, 99+%). Stoichiometric mixtures of the reactants were weighed and ground in an agate mortar and heated to 500ºC for 5 h. After that, the samples were reground and sintered at 625 ºC for 12 h in air. Powder X-ray diffraction (XRD) patterns were recorded by a Bruker D2 Phaser diffractometer (Cu Kα radiation, λ = 1.5406 Å) for phase identification. The X-ray Photoelectron Spectra (XPS) of Cs 3d, Rb 3d, K 2p, Al 1s, O 1s, Te $3d_{5/2}$ and valence band (VB) were recorded by a PHI5000 VersaProbe II XPS instruments (ULVAC-PHI, Japan) (Monochromatic X-ray of Al K_α ,1486.6 eV) at SUT-NANOTEC-SLRI joint research facility, Synchrotron Light Research Institute (SLRI), Thailand. The binding energies drift due to charging effects were corrected using the position of the C1s as a reference at 284.8

eV.[7-8] Agilent UV-Vis-NIR spectrophotometer modeled Carry 5000 was used for optical diffuse reflectance spectroscopy (DRS). The diffuse reflectance (%R) spectra were recorded in the wavelength range of 200-2000 nm with the double beam mode. Band gap energy was obtained by extrapolation of the plot of $(K\nu)^{1/2}$ versus photon energy (ν), where K is reflectance transformed according to Kubelka–Munk function [$K = (1 - R)^2/2(R)$], where $R = (\%R_{sample}/\%R_{standard})$.[9-10] The Electrical conductivity of all sintered samples was measured from 300 to 673 K by four-probe method using Keysight B2901A source/measure unit.

Calculations

The density of states (DOS) were calculated based on density functional theory (DFT) using the Vienna *ab initio* simulation package (VASP)[11-12] employing the Perdew, Burke, Ernzerhof (PBE) exchange-correlation function[13] implemented with the projector augmented-wave method (PAW).[14-15] Γ-centered 3×3×2 Monkhorst-Pack k-mesh was used for the Brillouin zone integrations. The cutoff energy for plane-wave basis sets was set at 520 eV. Structural relaxation was performed until the force on each ion is less than 0.01 eV/Å.

Results and discussions

Structure

Powder X-ray diffraction patterns indicate that all samples are single phase (Fig. 1). All diffractions can be indexed as AB_2O_6 defect cubic pyrochlore structure (β-pyrochlore) with $Fd\bar{3}m$ space group.[16] The defect pyrochlore structure can be explained based on the interpenetrating network of $(Al,Te)_2O_6$ corner sharing octahedral units with A cations (Cs, Rb, and K) occupying the interstitial sites. Comparing to $A_2B_2O_7$ pyrochlore, defect pyrochlore structure has lots of vacancies. In addition, there are few possible crystallographic sites for A cations. The XRD patterns in this work suggest no indication of them being at positions other than the normal 8b but small deviation from this ideal position, like the 32e position, is possible.

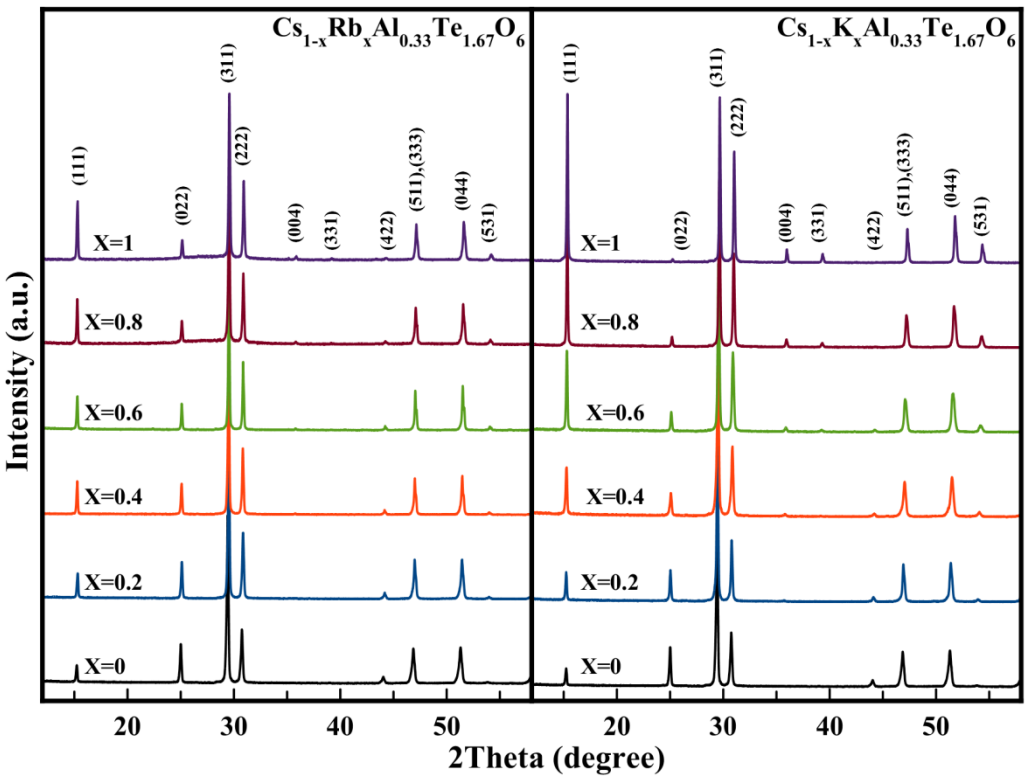

Fig. 1 XRD patterns of $Cs_{1-x}Rb_xAl_{0.33}Te_{1.67}O_6$ and $Cs_{1-x}K_xAl_{0.33}Te_{1.67}O_6$

It is worth to note that the displacive disorder of A cation from 8b to 32e position result in a nonlinear increase of cell parameters in $AAl_{0.33}W_{1.67}O_6$; A = Cs, Rb, and K.[17] However, such anomaly is not observed in this work although the samples are quite similar. Plots of calculated cell parameters versus substituting content are linear in both series (Fig. 2). As both K^+ (1.51 Å) and Rb^+ (1.61 Å) are smaller than Cs^+ (1.74 Å), increasing their content results in smaller cell parameters as expected.[18-19] However, the main network of the structure is the B_2O_6 octahedral network, changing A cations has a much smaller effect on the cell parameters comparing to changing the B cations. Similar results were reported by Castro and Rasines.[20]

XPS results

XPS survey spectra of $CsAl_{0.33}Te_{1.67}O_6$ (CATO), $RbAl_{0.33}Te_{1.67}O_6$ (RATO), and $KAl_{0.33}Te_{1.67}O_6$ (KATO) show the corresponding elemental compositions in each compound (Fig. 3). Cs3d, Rb3d and K2p XPS spectra in Fig. 4 give semi-quantitative results on the composition of the prepared samples. The obtained binding energies are close to those reported in literature.[21-24] The trend in peak areas of each element in the samples agrees well with their nominal composition.

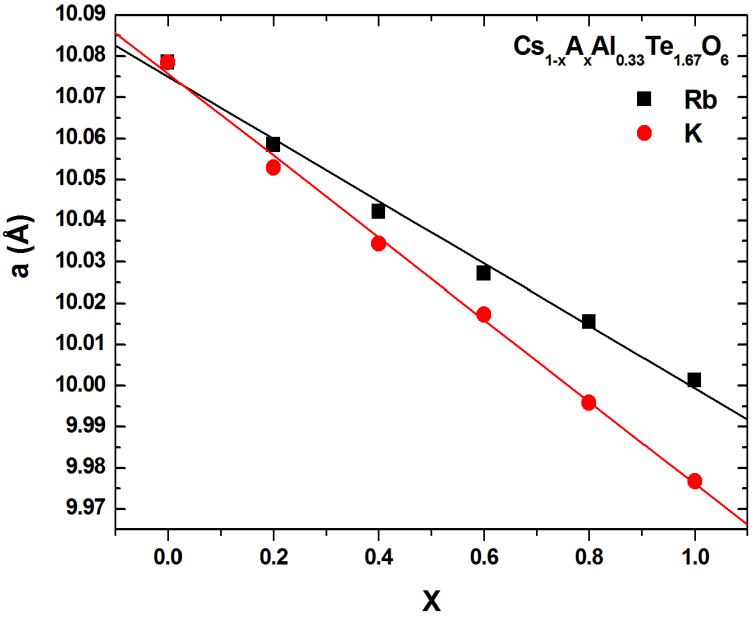

Fig. 2 Plots of cell parameters versus Rb and K content

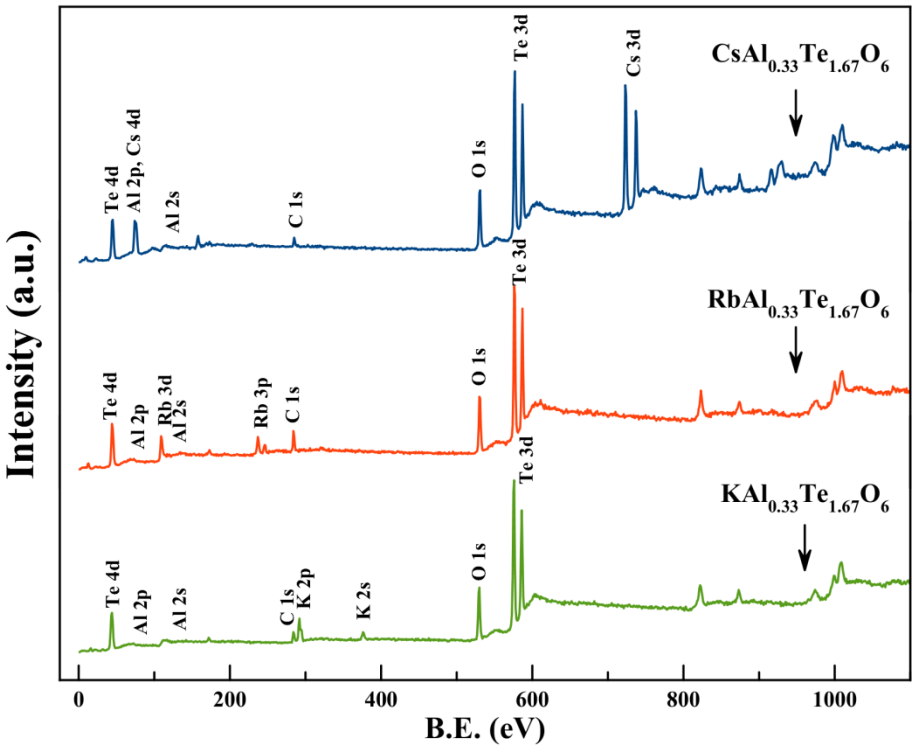

Fig. 3 XPS survey spectra of CATO, RATO, and KATO

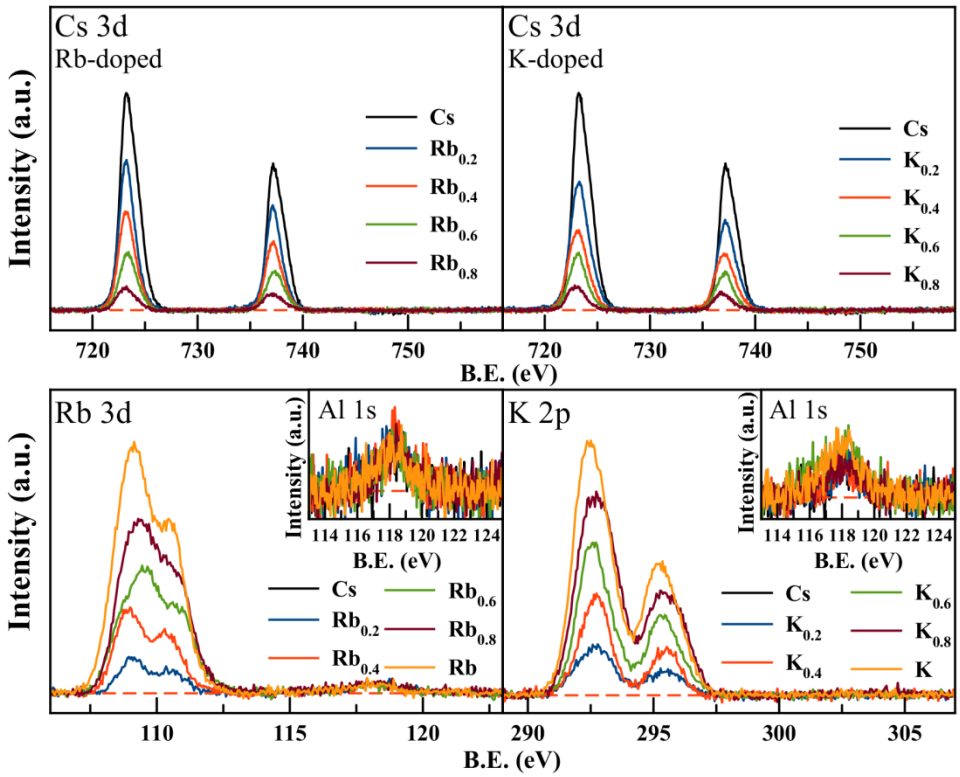

Fig. 4 Cs 3d, Rb 3d, K 2p and Al 1s XPS spectra of $Cs_{1-x}Rb_xAl_{0.33}Te_{1.67}O_6$ and $Cs_{1-x}K_xAl_{0.33}Te_{1.67}O_6$

XPS spectra of Te3 $d_{5/2}$ are also examined to probe oxidation states of Te in the samples. As seen in Fig. 5, all spectra show small asymmetry with a tail on the lower energy region. These spectra are fitted using two Gaussian-Lorentzian peaks; one represents Te^{4+}at lower binding energy and the other represents Te^{6+}. For comparison, $Te3d_{5/2}$ spectra of (CTO), a known compound which contains both $Te^{4+}$and Te^{6+}, are also shown and fitted with the same method here. The binding energy and peak area of each peak are summarized in Table 1. It is interesting to note that while the binding energies of the observed Te^{6+} are close to the reported values, those of Te^{4+} in $Cs_{1-x}A_xAl_{0.33}Te_{1.67}O_6$ (A = K, Rb, and Cs) are slightly smaller than most reported values for Te^{4+}.[25-26] On the other hand, the obtained values are too high to be assigned to Te(0) or Te^{2-} states.[27] As chemical environments affect the binding energy, binding energy of Te^{4+} in these samples which is in the unique compressed octahedra is expected to be different from that of Te^{4+} in TeO_2 standard. In fact, our values are close to that reported in $Gd_2(Ti_{2-y}Te_y)O_7$ pyrochlores.[28]

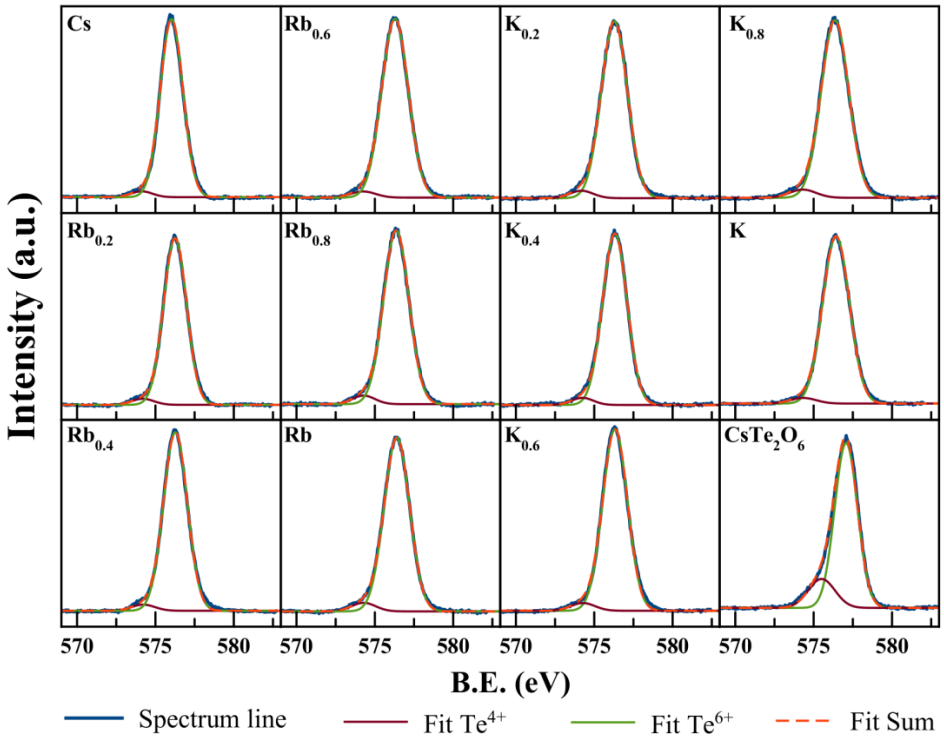

Fig. 5: XPS Te $3d_{5/2}$ spectra of the samples

It is difficult to quantitatively conclude the amount of Te^{4+} in the samples based solely on the peak areas. Nevertheless, the existence of $Te^{4+}$is obvious and its amount in the cubic pyrochlore samples is very low. The presence of small amount of Te^{4+} is a result of small deviation in stoichiometry as reported by Li et al.[6] who concluded that the composition of the prepared $CsAl_{0.33}Te_{1.67}O_6$ was actually $CsAl_{0.30}Te_{1.70}O_6$. Small amount of Te^{6+} must then be reduced to Te^{4+} to maintain charge neutrality. Te $3d_{5/2}$ XPS results reported here reveal the existence of Te^{4+} in all samples with similar peak areas suggesting that the Rb and K substituted samples contain similar defects with a similar amount.

Table 1: Te $3d_{5/2}$ fitting results

Comp. (X)	Te^{6+}		Te^{4+}		Ratio of Te^{6+}: Te^{4+} (1.67)	R^2
	B.E. (eV)	FWHM (eV)	B.E. (eV)	FWHM (eV)		
0	576.03	1.70	574.12	1.62	1.62:0.05	0.9983
Rb-doped						
0.2	576.25	1.72	574.19	1.68	1.61:0.06	0.9991
0.4	576.27	1.79	574.22	1.78	1.62:0.05	0.9987
0.6	576.28	2.00	574.25	1.86	1.62:0.05	0.9994
0.8	576.36	1.90	574.28	1.68	1.60:0.07	0.9992
1.0	576.40	1.85	574.28	1.80	1.60:0.07	0.9995
K-doped						
0.2	576.28	1.89	574.29	1.68	1.61:0.06	0.9993
0.4	576.32	1.79	574.33	1.72	1.60:0.07	0.9995
0.6	576.32	1.84	574.34	1.61	1.60:0.07	0.9982
0.8	576.35	2.02	574.43	1.99	1.60:0.07	0.9987
1.0	576.42	1.97	574.46	1.87	1.61:0.06	0.9992
$CsTe_2O_6$						
-	577.07	1.72	575.50	2.00	1.66:0.44 ($Te^{6+}_{1.5}$: $Te^{4+}_{0.5}$)	0.9981

XPS spectra at valence band region (Fig. 6a) give useful information regarding electronic structure of the samples. Like most oxides, the top of the valence band is predominantly O 2p. The outstanding feature of the spectra is the position of alkali p orbitals which is at about 10, 13, and 17 eV for Cs 5p, Rb 4p, and K 3p, respectively. The positions of these states are similar to values in other reports.[24, 29-30] Rb 4p and K 3p bands are quite separated from O 2p near the top of the valence band and should not have much contribution in it. Thus, the spectral feature and position of the valence band in Rb and K containing samples are very similar. This also implies that any effects from the difference in bond distances and angles are insignificant. Two samples containing Cs have similar spectra although there are some differences as both samples contain quite a different composition and have related, but different, crystal structure. As Cs 5p bands are clearly overlapping with O2p, Cs is believed to contribute to the valence band. The overlapping between Cs 5p and O 2p in the valence band is observed in many oxides.[31-32] The contribution from Cs 5p broadens the valence band thus causes the shift in its position comparing to the other two samples with no Cs. In addition, the spectral shape of CTO valence band is different from others. Besides the dominant peaks contributed by O 2p, there is another small peak on top of that the valence band maximum (VBM) (Fig. 6b).

To gain deeper understandings, band structure calculation was performed for CTO. Valence band of CTO may be divided into three regions (Fig. 6c). The small peaks at VBM consist of O 2p and Te 5s orbitals. The wide region at approximately -1 to -6 eV is predominantly O 2p with a small contribution from Te 4d orbital and the sharp peak at about -6 to -8 eV is formed mainly by Cs 5p orbital with some contribution from Te 5p. These main features of the valence band are qualitatively comparable to the obtain XPS spectra. It is interesting to note that the small peak at VBM is not observed in XPS spectra of the $AAl_{0.33}Te_{1.67}O_6$ series. However, as proposed by Li et al.[6] and deduced from $Te3d_{5/2}$ spectra, $AAl_{0.33}Te_{1.67}O_6$ samples should contain only about 3% of Te^{4+} which is very little comparing to 25% in CTO. Besides, it is difficult to compare the spectra of these two series as they have a different structure which leads to the different position of Te 5s.

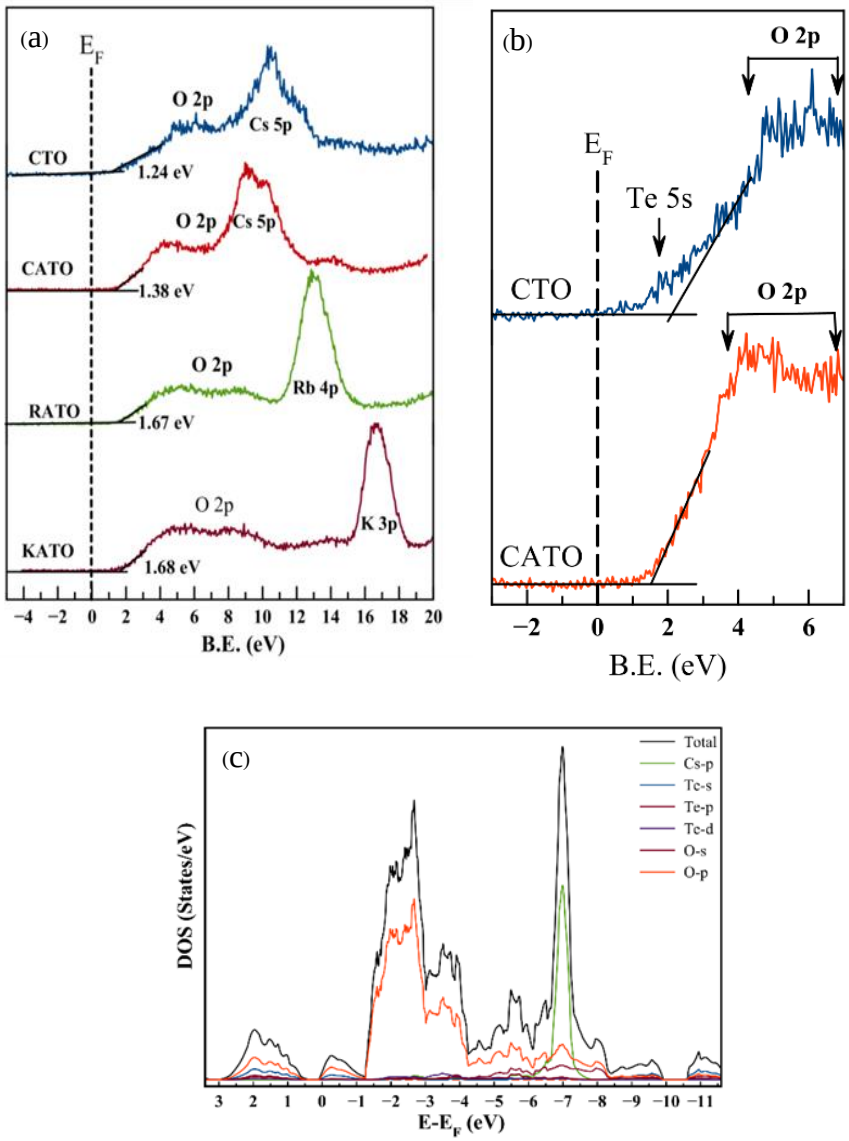

Fig. 6 XPS valence band spectra of $CsTe_2O_6$ and $AAl_{0.33}Te_{1.67}O_6$ (A = Cs, Rb, and K) (a) and the close-up of Cs containing samples showing an additional small peak near the Fermi level (b). (c) shows the calculated valence band of $CsTe_2O_6$.

Electrical properties

Electronic conductivity of $Cs_{1-x}A_xAl_{0.33}Te_{1.67}O_6$, A = Rb and K decrease with increasing A content. The effect is very significant as room temperature conductivity of $KAl_{0.33}Te_{1.67}O_6$and $RbAl_{0.33}Te_{1.67}O_6$ are 10^3 and 10^5 times lower than that of $CsAl_{0.33}Te_{1.67}O_6$, respectively (Fig. 7). Conductivity of all samples are plotted based on Arrhenius' equation: $\sigma = Ae^{(-Ea/kT)}$ where A is pre-exponential constant, k is Boltzmann constant, Ea is activation energy, and T is absolute temperature as shown in Fig. 7 and the activation energy are

calculated and summarized in Table 2. It is obvious that the lower Cs content, the higher the activation energy. Interestingly, Siritanon et. al.[5] previously reported that the Arrhenius plot of $Cs(M,Te)_2O_6$ are not linear in temperature range 50-300 K and concluded that the samples exhibit variable range hopping conduction as the plots of log conductivity vs. $1/T^{1/4}$ are linear. Therefore, the samples have different conduction processes at different temperatures. In fact, crossover from variable range hopping conduction to thermally activated band conduction from low to high temperatures have been reported in many systems and believed to also be the case here.[33-34]

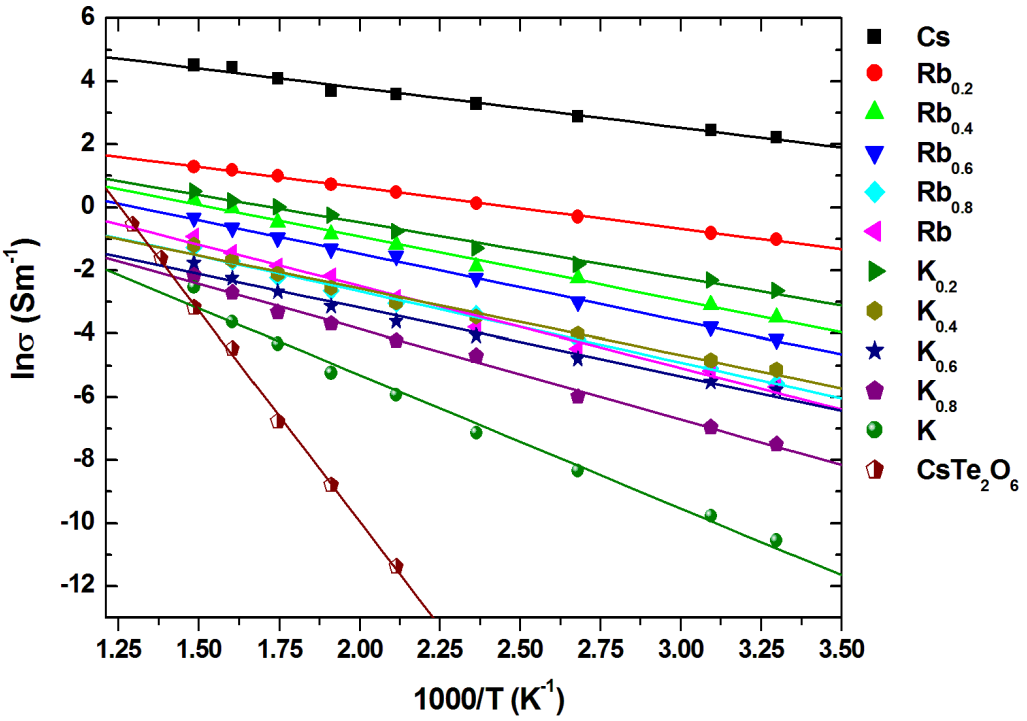

Fig. 7 Electronic conductivity of $Cs_{1-x}A_xAl_{0.33}Te_{1.67}O_6$ (A = Rb and K) and $CsTe_2O_6$ samples fitted with Arrhenius equation.

Table 2: Activation energy and R^2 obtained from fitting the electronic conductivity of $Cs_{1-x}A_xAl_{0.33}Te_{1.67}O_6$; A = Rb and K and $CsTe_2O_6$ with Arrhenius equation.

x	E_a (eV)	R^2	x	E_a (eV)	R^2
0	0.108	0.9854	$CsTe_2O_6$	1.15	0.9987
Rb-doped			**K-doped**		
0.2	0.113	0.9985	0.2	0.151	0.9914
0.4	0.174	0.9921	0.4	0.180	0.9856
0.6	0.183	0.9972	0.6	0.186	0.9855
0.8	0.194	0.9919	0.8	0.247	0.9934
1.0	0.224	0.9870	1.0	0.364	0.9888

Optical property

The UV-Vis absorption spectra of CTO and $AAl_{0.33}Te_{1.67}O_6$, A = Cs, Rb, and K is shown in Fig. 8a and the band gap energy obtained from the extrapolations (Fig. 8b) are summarized in Fig. 9. Although most oxides containing Cs and Te have large band gap and white color, the band gap of CTO is only about 1.4 eV and the compound is dark brown. The unusually small band gap is a result of Te^{4+}, Te^{6+} intervalence charge transfer (IVCT) which gives rise to the absorption in a visible region corresponding to the transition from Te^{4+} $5s^2$ to Te^{6+} $5s^0$. Although there are very few reports on Te^{4+}/Te^{6+} charge transfer, similar mechanism is widely studied in other mixed valence systems including those with post transition cations like Sb, Sn, Tl.[35-36]

UV-Vis spectra of $AAl_{0.33}Te_{1.67}O_6$ series are obviously different from that of CTO although the compounds also containTe^{4+}/Te^{6+} mixed valency. However, Te^{4+} and Te^{6+} in CTO are in different crystallographic sites while those in $AAl_{0.33}Te_{1.67}O_6$ are in the same one. As λ_{max} of absorption should be directly related to the energy difference between Te^{4+} $5s^2$ and Te^{6+} $5s^0$, the more similarity of the environment around Te^{4+} and Te^{6+} in $AAl_{0.33}Te_{1.67}O_6$ results in absorptions at a longer wavelength. Therefore, it is concluded here that the very

broad and strong absorption centering at long wavelengths is associated with IVCT of Te^{4+} and Te^{6+}. Mizoguchi et al.[35] also reported similar diffuse reflectance spectra of $BaSn_{1-x}Sb_xO_3$ which contain mixed valence ions and show a very broad absorption band due to IVCT.

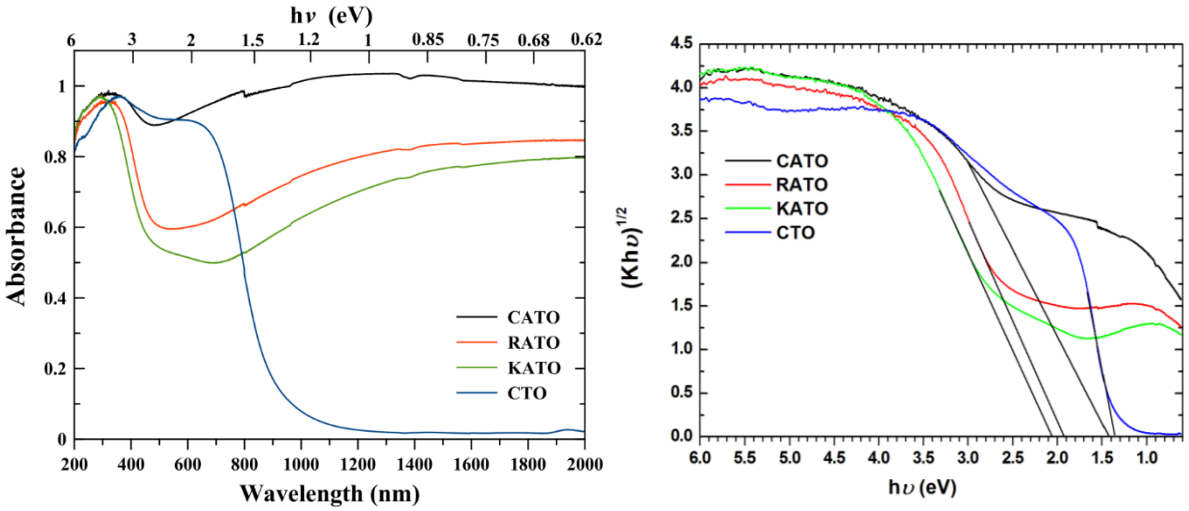

Fig. 8: UV-Vis spectra (a) and extrapolation of the band gap energy (b) of $CsTe_2O_6$ and $AAl_{0.33}Te_{1.67}O_6$ (A = Cs, Rb, and K)

Discussions

It has been established that $CsAl_{0.33}Te_{1.67}O_6$ shows relatively high conductivity.[5] Li et. al.[6] concluded that the conductivity comes from small deviations from stoichiometry which results in small amount of Te^{4+} producing mixed valence compounds. The n-type behavior in these series of compounds is explained by the presence of donor defect levels originating from Te^{4+}. In general, type of M cations in $Cs(M,Te)_2O_6$ affects the conductivity of the compounds as small M cation reduces M/Te-O distance thus destabilizes Te^{4+} in the structure increasing their energy level. In addition, some M cations could provide orbitals with appropriate energy to overlap with Te 5s which increase the conductivity.

When Cs is replaced by Rb and K in $Cs_{1-x}A_xAl_{0.33}Te_{1.67}O_6$, the difference in conductivity is very pronounced although the same Al is present. Additionally, samples containing Rb and K have much less conductivity despite the smaller cell parameters. XPS results obtained in this work do not indicate any difference in the number of Te^{4+}, hence the number of defect levels, in all samples. In addition, we have also prepared and measured conductivity of $CsAl_xTe_{2-x}O_6$ and $RbAl_xTe_{2-x}O_6$ with different x values. As shown in Fig. S1, the conductivity of both series exhibit similar Al content dependency which is also in

agreement with the previous work.[6] It is, therefore, reasonable to conclude that the type and the amount of defect, e.g. Te^{4+}, are similar in all samples. If the number of Te^{4+} is similar, then the difference in conductivity must be related toTe^{4+} energy level relative to the conduction band.

Based on the band gap energy obtained from UV-Vis results and the VBM position obtained from XPS valence band spectra, we propose schematic band structure diagram of the samples as depicted in Fig. 9. From the figure, the difference between Fermi energy level and the bottom of the conduction band (E_d) is obtained. Generally, the band diagrams of these four samples represent their semiconducting behavior. However, the activation energies of conduction indicate that their behavior are different. The activation energy of conduction of CTO (1.15 eV) (Fig.7) is in the same order with its band gap energy suggesting the intrinsic semiconducting behavior. The conductivity of this sample is small because large energy is required to activate electrons across the band gap. It is noteworthy that E_d and the activation energy of conduction in CTO are significantly different which indicates that there is no defect level at the Fermi energy level (E_F). On the other hand, the activation energies of $AAl_{0.33}Te_{1.67}O_6$ are close to E_d and much smaller than their band gap energy which suggests the presence of defect levels close to the conduction band within the band gap. The presence of such defect levels is a characteristic of n-type semiconductors which agrees well with the negative Seebeck coefficients.[5] E_d in these three samples indicate the position of defect levels relative to conduction band minimum (CBM) which determines conductivity of the samples.

Replacing Cs with Rb and K have two effects on the band diagram; lowering the VBM and increasing the band gap energy. It should be noted that lowering VBM in these cases is not the only cause of increasing the band gap. Without the presence of Cs, VBM of both RATO and KATO is about 0.3 eV lower in energy. However, the band gap differences between the samples are 0.5-0.6 eV. As the conduction band should be mainly Te 5s with some contribution from Al and O, Te/Al-O bond distance and Te/Al-O-Te/Al bond angle must play important roles in determining the CBM. Additional detail studies are required to further explain this matter. Nevertheless, the combination of VBM lowering and band gap energy increasing when Cs is replaced with Rb and K result in larger E_d and consequently lower conductivity.

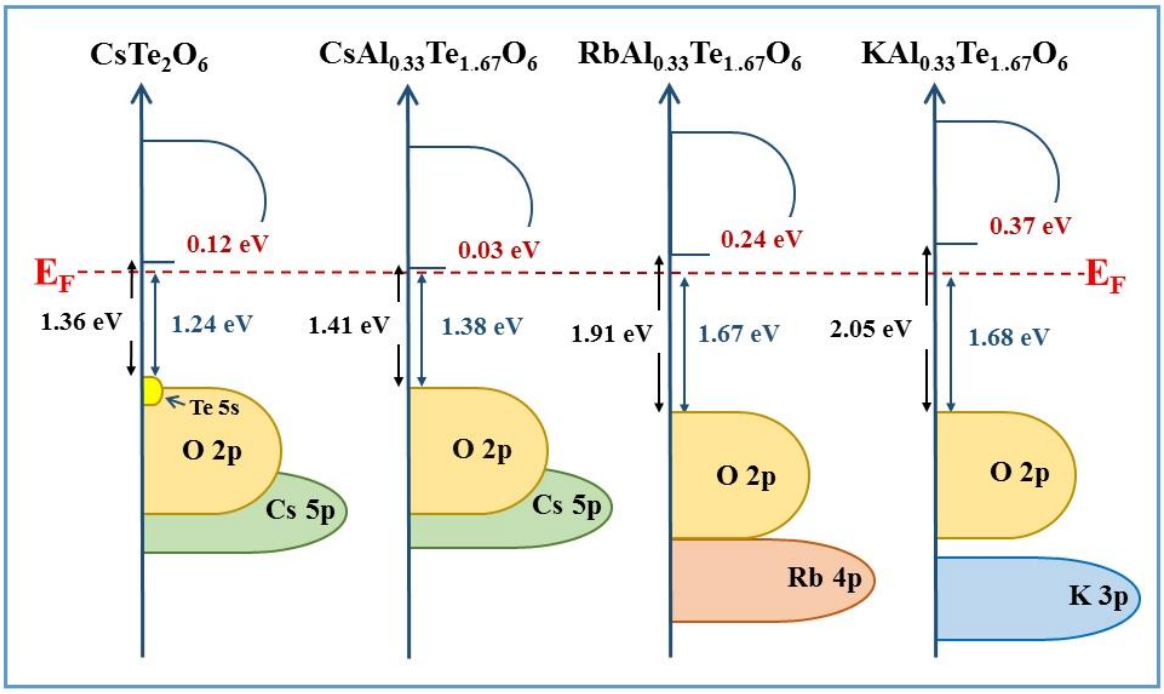

Compounds	Valence band position (eV)	Band gap energy (eV)	E_a (eV)	Activation energy of conduction (eV)
$CsTe_2O_6$	1.24	1.36	0.12	1.15
$CsAl_{0.33}Te_{1.67}O_6$	1.38	1.41	0.03	0.108
$RbAl_{0.33}Te_{1.67}O_6$	1.67	1.91	0.24	0.224
$KAl_{0.33}Te_{1.67}O_6$	1.68	2.05	0.37	0.364

Fig. 9 Schematic band structures of $CsTe_2O_6$ and $AAl_{0.33}Te_{1.67}O_6$ (A = Cs, Rb, and K)

Acknowledgements

This work is financially supported by The Thailand Research Fund and Suranaree University of Technology, Thailand (Grant No. TRG5780068). We thank the synchrotron light research institute (public organization), Thailand, especially SUT-NANOTEC-SLRI joint research facility, for XPS facilities. We also gratefully acknowledge S. Jungthawan for useful discussions on calculation methods.

Supporting Information: 1. Figure showing the resistivity of $AAl_xTe_{2-x}O_6$ (A = Cs and Rb).

Reference

1. Kawazoe, H.; Yanagi, H.; Ueda, K.; Hosono, H., Transparent p-type conducting oxides: design and fabrication of pn heterojunctions. *Mrs Bull.* **2000**, *25*, 28-36.
2. Noguchi, S.; Sakata, H., Electrical properties of undoped In_2O_3 films prepared by reactive evaporation. *J. Phys. D: Appl. Phys.* **1980**, *13*, 1129.
3. Cai, S.; Li, Y.; Chen, X.; Ma, Y.; Liu, X.; He, Y., Optical and electrical properties of Ta-doped ZnSnO3 transparent conducting films by sol–gel. *J. Mater. Sci: Mater. Electron.* **2016**, *27*, 6166-6174.
4. O'Neil, D. H.; Kuznetsov, V. L.; Jacobs, R. M.; Jones, M. O.; Edwards, P. P., Structural, optical and electrical properties of $In_4Sn_3O_{12}$ films prepared by pulsed laser deposition. *Mater. Chem. Phys.* **2010**, *123*, 152-159.
5. Siritanon, T.; Laurita, G.; Macaluso, R. T.; Millican, J. N.; Sleight, A. W.; Subramanian, M., First observation of electronic conductivity in mixed-valence tellurium oxides. *Chem. Mater.* **2009**, *21*, 5572-5574.
6. Li, J.; Siritanon, T.; Stalick, J. K.; Sleight, A. W.; Subramanian, M., Structural studies and electrical properties of Cs/Al/Te/O phases with the pyrochlore structure. *Inorg. Chem.* **2011**, *50*, 5747-5754.
7. Howng, W.-Y.; Thorn, R., Investigation of the electronic structure of $La_{1-x}(M^{2+})_xCrO_3$, Cr_2O_3 and La_2O_3 by X-ray photoelectron spectroscopy. *J. Phys. Chem. Solids.* **1980,** *41*, 75-81.
8. Lv, Y.; Yao, W.; Zong, R.; Zhu, Y., Fabrication of Wide–Range–Visible Photocatalyst Bi_2WO_{6-x} nanoplates via Surface Oxygen Vacancies. *Sci. Rep.* **2016**, *6*, 19347.
9. Guje, R.; Ravi, G.; Palla, S.; Rao, K. N.; Vithal, M., Synthesis, characterization, photocatalytic and conductivity studies of defect pyrochlore $KM_{0.33}Te_{1.67}O_6$ (M= Al, Cr and Fe). *Mater. Sci. Eng. B* **2015**, *198*, 1-9.
10. Morales, A. E.; Mora, E. S.; Pal, U., Use of diffuse reflectance spectroscopy for optical characterization of un-supported nanostructures. *Rev. Mex. Fis. S* **2007**, *53*, 18.
11. Kresse, G.; Hafner, J., Ab initiomolecular dynamics for open-shell transition metals. *Phys. Rev. B* **1993**, *48*, 13115-13118.
12. Fuchs, F.; Furthmüller, J.; Bechstedt, F.; Shishkin, M.; Kresse, G., Quasiparticle band structure based on a generalized Kohn-Sham scheme. *Phys. Rev. B* **2007**, *76*, 115109.
13. Perdew, J. P.; Burke, K.; Ernzerhof, M., Generalized Gradient Approximation Made Simple. *Phys. Rev. Lett.* **1996**, *77*, 3865-3868.

14. Blöchl, P. E., Projector augmented-wave method. *Phys. Rev. B* **1994**, *50*, 17953-17979.

15. Kresse, G.; Joubert, D., From ultrasoft pseudopotentials to the projector augmented-wave method. *Phys. Rev. B* **1999,** *59*, 1758-1775.

16. Subramanian, M.; Aravamudan, G.; Rao, G. S., Oxide pyrochlores-a review. *Prog. Solid State Chem.* **1983**, *15*, 55-143.

17. Thorogood, G. J.; Kennedy, B. J.; Peterson, V. K.; Elcombe, M. M.; Kearley, G. J.; Hanna, J. V.; Luca, V., Anomalous lattice parameter increase in alkali earth aluminium substituted tungsten defect pyrochlores. *J. Solid State Chem.* **2009**, *182*, 457-464.

18. Shannon, R. T.; Prewitt, C. T., Effective ionic radii in oxides and fluorides. *Acta Crystallogr. B* **1969**, *25*, 925-946.

19. Shannon, R. t., Revised effective ionic radii and systematic studies of interatomic distances in halides and chalcogenides. *Acta Crystallogr. A* **1976**, *32*, 751-767.

20. Castro, A.; Rasines, I.; Turrillas, X., Synthesis, X-ray diffraction study, and ionic conductivity of new AB_2O_6 pyrochlores. *J. Solid State Chem.* **1989**, *80*, 227-234.

21. Marschall, R.; Mukherji, A.; Tanksale, A.; Sun, C.; Smith, S. C.; Wang, L.; Lu, G. Q. M., Preparation of new sulfur-doped and sulfur/nitrogen co-doped $CsTaWO_6$ photocatalysts for hydrogen production from water under visible light. *J. Mater. Chem.* **2011**, *21*, 8871-8879.

22. Guo, C.; Yin, S.; Dong, Q.; Sato, T., Near-infrared absorption properties of Rb_xWO_3 nanoparticles. *CrystEngComm* **2012**, *14*, 7727-7732.

23. Ravi, G.; Veldurthi, N. K.; Palla, S.; Velchuri, R.; Pola, S.; Reddy, J. R.; Vithal, M., Synthesis, characterization and photocatalytic activity of $KAl_{0.33}W_{1.67}O_6$ and $Sn_{0.5}Al_{0.33}W_{1.67}O_6\,xH_2O$. *Photochem. Photobiol.* **2013**, *89*, 824-831.

24. Atuchin, V.; Kesler, V.; Meng, G.; Lin, Z., The electronic structure of $RbTiOPO_4$ and the effects of the A-site cation substitution in $KTiOPO_4$-family crystals. *J. Phys. Condens. Matter.* **2012**, *24*, 405503.

25. Sathiya, M.; Ramesha, K.; Rousse, G.; Foix, D.; Gonbeau, D.; Guruprakash, K.; Prakash, A.; Doublet, M.; Tarascon, J.-M., Li_4NiTeO_6 as a positive electrode for Li-ion batteries. *Chem. Commun.* **2013**, *49*, 11376-11378.

26. Tan, G.; Zhang, X.; Chen, Z., Colossal magnetoresistance effect of electron-doped manganese oxide thin film $La_{1-x}Te_xMnO_3$ (x= 0.1, 0.15). *J. Appl. Phys.* **2004**, *95*, 6322-6324.

27. Sartz Jr, W. E.; Wynne, K. J.; Hercules, D. M., X-ray photoelectron spectroscopic investigation of Group VIA elements. *Anal. Chem.* **1971**, *43*, 1884-1887.

28. Heredia, A.; García, M. Q.; Mazariego, J. P.; Escamilla, R., X-ray diffraction and Raman spectroscopy on $Gd_2(Ti_{2-y}Te_y)O_7$ prepared at high pressure and high temperature. *J. Alloy Compd.* **2010**, *504*, 446-451.

29. Slobodin, B.; Surat, L.; Zubkov, V.; Tyutyunnik, A.; Berger, I.; Kuznetsov, M.; Perelyaeva, L.; Shein, I.; Ivanovskii, A.; Shulgin, B., Structural, luminescence, and electronic properties of the alkaline metal-strontium cyclotetravanadates $M_2Sr\ (VO_3)_4$,(M= Na, K, Rb, Cs). *Phys. Rev. B* **2005**, *72*, 155205.

30. Van den Berghe, S.; Laval, J.-P.; Gaudreau, B.; Terryn, H.; Verwerft, M., XPS investigations on cesium uranates: mixed valency behaviour of uranium. *J. nucl. mater.* **2000**, *277*, 28-36.

31. Waghmode, S. B.; Vetrivel, R.; Hegde, S. G.; Gopinath, C. S.; Sivasanker, S., Physicochemical investigations of the basicity of the cation exchanged ETS-10 molecular sieves. *J. Phys. Chem. B* **2003**, *107*, 8517-8523.

32. Yang, Y.; Su, X.; Pan, S.; Zhang, M.; Wang, Y.; Han, J.; Yang, Z., Crystal growth and calculation of the electronic band structure and density of states of $Li_3Cs_2B_5O_{10}$. *CrystEngComm* **2014**, *16*, 1978-1984.

33. Han, M.; Jiang, K.; Zhang, J.; Yu, W.; Li, Y.; Hu, Z.; Chu, J., Structural, electronic band transition and optoelectronic properties of delafossite $CuGa_{1-x}Cr_xO_2$ ($0 \leq x \leq 1$) solid solution films grown by the sol–gel method. *J. Mater. Chem.* **2012**, *22*, 18463-18470.

34. Okutan, M.; Bakan, H. I.; Korkmaz, K.; Yakuphanoglu, F., Variable range hopping conduction and microstructure properties of semiconducting Co-doped TiO_2. *Phys. B Condens. Matter* **2005**, *355*, 176-181.

35. Mizoguchi, H.; Chen, P.; Boolchand, P.; Ksenofontov, V.; Felser, C.; Barnes, P. W.; Woodward, P. M., Electrical and optical properties of Sb-doped $BaSnO_3$. *Chem. Mater.* **2013**, *25*, 3858-3866.

36. Atkinson, L.; Day, P., Charge transfer in mixed-valence solids. Part IV. Electronic spectra of hexachloroantimonates (III, V). *J. Chem. Soc. A* **1969**, 2423-2431.

Table of Contents graphic AND synopsis

Synopsis: Complete solid solutions of K and Rb doped $CsAl_{0.33}Te_{1.67}O_6$ were prepared and studied. While possess the same structure and similar Te^{4+}/Te^{6+} mixed valency, replacing Cs with Rb and K greatly reduce the conductivity of $CsAl_{0.33}Te_{1.67}O_6$. The schematic band structures of the compounds are proposed based on XPS and absorption results and used to explain the electrical conductivity of the compounds.

"For Table of Contents Only"

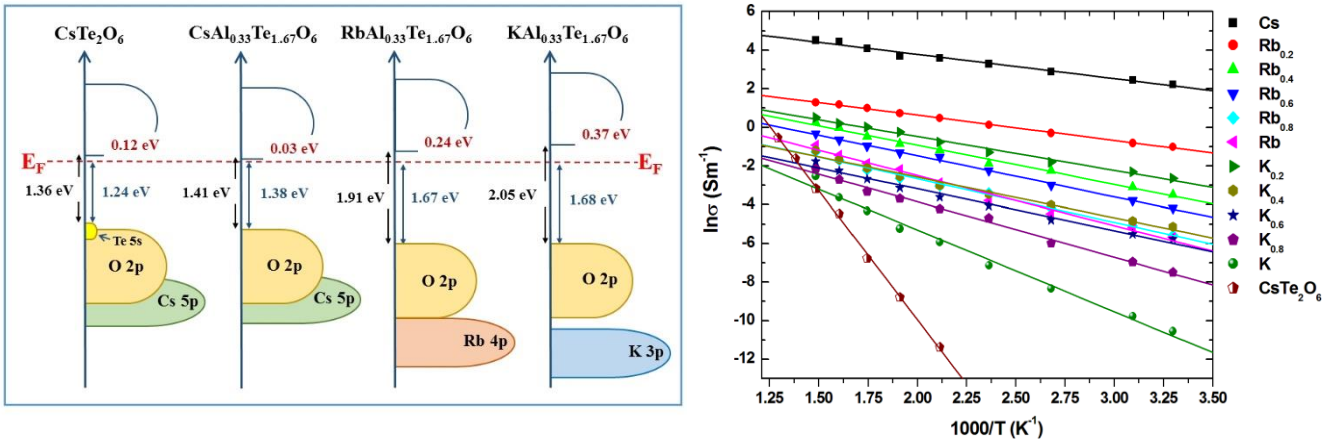

Supporting Information

Electrical properties of $AAl_{0.33}Te_{1.67}O_6$ (A = K, Rb, and Cs) mixed valence pyrochlores

Anurak Waehayee[a], Tanachat Eknapakul[b],Narong Chanlek[c],Thanundon Kongnok[b], Surachet Rattanasuporn[c], Hideki Nakajima[c], Worawat Meevasana[b,d,e], Theeranun Siritanon[a,d,e]*

[a]School of Chemistry, Institute of Science, 111 University Avenue, Muang,Suranaree University of Technology 30000, Thailand

[b]School of Physics, Institute of Science, Suranaree University of Technology 30000, Thailand

[c]Synchrotron Light Research Institute, Nakhon Ratchasima 30000, Thailand

[d]NANOTEC-SUT Center of Excellence on Advanced Functional Nanomaterials, Suranaree University of Technology, Nakhon Ratchasima 30000, Thailand

[e]Center of Excellence-Advanced Functional Materials, Suranaree University of Technology

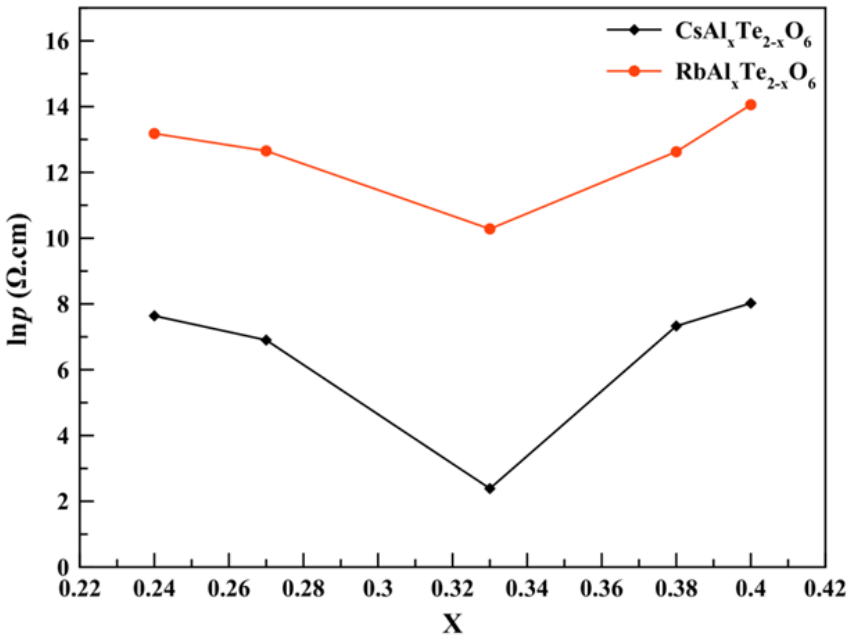

Fig. S1 Resistivity of the $AAl_xTe_{2-x}O_6$ (A = Cs and Rb). Note that resistivity of $KAl_xTe_{2-x}O_6$ samples when x is not equal to 0.33 are too high to be measured with the current technique.

Journal of Alloys and Compounds 718 (2017) 215–222

Contents lists available at ScienceDirect

Journal of Alloys and Compounds

journal homepage: http://www.elsevier.com/locate/jalcom

Electrical properties of $(Cs_{1-x}A_x)Al_{0.33}Te_{1.67}O_6$ (A = K and Rb) mixed valence pyrochlores

Anurak Waehayee [a], Tanachat Eknapakul [b], Narong Chanlek [c], Thanundon Kongnok [b], Surachet Rattanasuporn [c], Hideki Nakajima [c], Worawat Meevasana [b, d, e], Theeranun Siritanon [a, d, e, *]

[a] School of Chemistry, Institute of Science, Suranaree University of Technology, Nakhon Ratchasima, 30000, Thailand
[b] School of Physics, Institute of Science, Suranaree University of Technology, Nakhon Ratchasima, 30000, Thailand
[c] Synchrotron Light Research Institute, Nakhon Ratchasima, 30000, Thailand
[d] NANOTEC-SUT Center of Excellence on Advanced Functional Nanomaterials, Suranaree University of Technology, Thailand
[e] Center of Excellence-Advanced Functional Materials, Suranaree University of Technology, Thailand

ARTICLE INFO

Article history:
Received 6 March 2017
Received in revised form
28 April 2017
Accepted 3 May 2017
Available online 6 May 2017

Keywords:
Oxide
Mixed valence compounds
Electrical properties
X-ray photoelectron spectroscopy

ABSTRACTS

The preparation and electronic properties of $Cs_{1-x}A_xAl_{0.33}Te_{1.67}O_6$ (A = K, Rb, and Cs) are reported. Replacing Cs with smaller Rb and K reduces cell parameters of the compounds but does not affect the overall structure. Electronic conductivities of all samples were measured and explained based on the band conduction model. Although XPS $Te3d_{5/2}$ spectra indicate that all samples contain similar amount of Te^{4+}/Te^{6+} mixed valency, their conductivities are varied from about 0.1 S cm in $CsAl_{0.33}Te_{1.67}O_6$ to 3×10^{-5} S cm in $RbAl_{0.33}Te_{1.67}O_6$ and 3×10^{-7} S cm in $KAl_{0.33}Te_{1.67}O_6$ at 300 K. To explain such large differences, the band structure diagrams are proposed based on the UV–Vis spectra and XPS spectra at valence band region. When the obtained activation energies of conduction and the proposed band diagram are considered, it is concluded that $AAl_{0.33}Te_{1.67}O_6$ (A = K, Rb, and Cs) are n-type semiconductors. The defect levels in these samples originate from Te^{4+} whose energy level relative to the conduction band minimum is different from samples to samples. Such differences are affected by Cs content in the structure as Cs seems to lower the band gap energy and increase the valence band maximum. It is the position of these defect levels that determines the electronic conductivity of the compounds.

1. Introduction

Post transition elements form oxides with interesting structures and properties. Several oxides containing heavy post-transition elements are known to have good electronic conductivity due to the presence of diffused s orbitals which results in wide conduction bands and low carrier mobility [1]. Some well-known examples include In_2O_3, $ZnSnO_3$, and $In_4Sn_3O_{12}$ [2-4]. However, conducting tellurium oxides are very rare. To our knowledge, the only clear examples are series of defect pyrochlores with general formula $Cs(M,Te)_2O_6$; M = 2+, 3+ and 4+ cations which show n-type semiconducting behavior due to Te^{4+}/Te^{6+} mixed valency [5].

It has been established that M cations in the mentioned formula play some roles in determining the electronic conductivities of the compounds. Smaller M cations reduce the cell parameter which compresses Te^{4+} in the structure and consequently destabilizes it. In addition, suitable M cations could provide orbitals with appropriate energy to overlap with Te 5s which could give rise to samples with higher conductivity. Only one compound in the series, $Cs(Al,Te)_2O_6$, was extensively investigated through detailed structural studies where it was concluded that Te^{4+}/Te^{6+} mixed valency in the compounds is a result of small deviations from stoichiometry [6]. However, the role of Cs in the structure remains unclear. Thus, the objectives of this work are to deepen the understanding of these series of oxides and to study the effects of cations at Cs position on the electronic properties of compounds in $Cs_{1-x}A_xAl_{0.33}Te_{1.67}O_6$; A = Rb and K series.

* Corresponding author. School of Chemistry, Institute of Science, Suranaree University of Technology, Nakhon Ratchasima, 30000, Thailand.
E-mail address: theeranun@sut.ac.th (T. Siritanon).

http://dx.doi.org/10.1016/j.jallcom.2017.05.025
0925-8388/

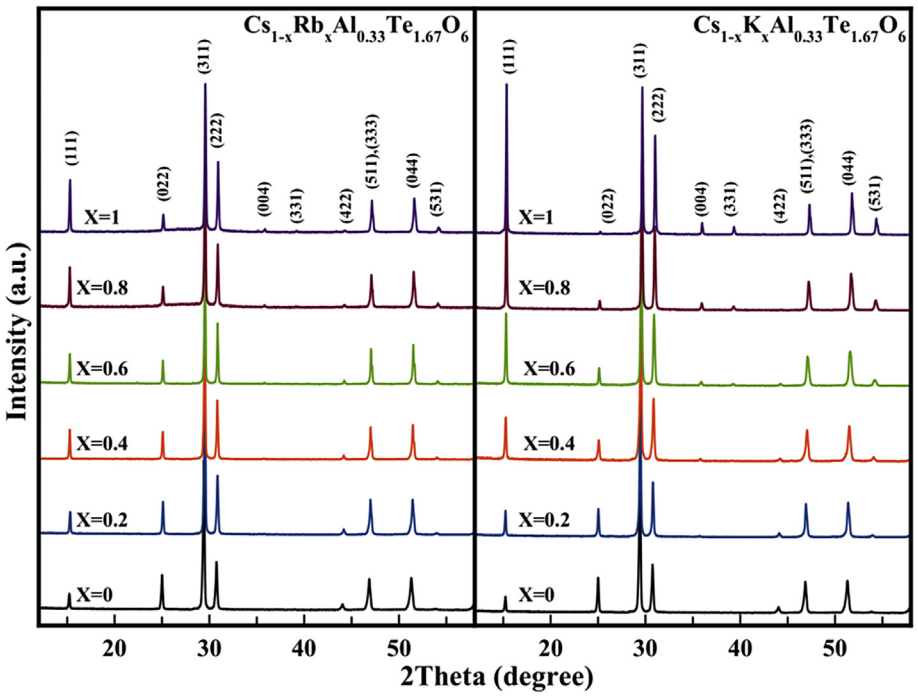

Fig. 1. XRD patterns of $Cs_{1-x}Rb_xAl_{0.33}Te_{1.67}O_6$ and $Cs_{1-x}K_xAl_{0.33}Te_{1.67}O_6$.

2. Experimental section

All samples were prepared by solid state reaction. The reactants were $CsNO_3$ (Sigma-Aldrich, 99+%), $RbNO_3$ (Acros organic, 99.8%), Al_2O_3 (Acros organic, 99+ %, for Rb-doped series), $Al(OH)_3$ (Acros organic, 99.9%, for K-doped series) and TeO_2 (Acros organic, 99+%). Stoichiometric mixtures of the reactants were weighed and ground in an agate mortar and heated to 500 °C for 5 h. After that, the samples were reground and sintered at 625 °C for 12 h in air. Powder X-ray diffraction (XRD) patterns were recorded by a Bruker D2 Phaser diffractometer (Cu Kα radiation, λ = 1.5406 Å) for phase identification. The X-ray Photoelectron Spectra (XPS) of Cs 3d, Rb 3d, K 2p, Al 1s, O 1s, Te $3d_{5/2}$ and valence band (VB) were recorded by a PHI5000 VersaProbe II XPS instruments (ULVAC-PHI, Japan) (Monochromatic X-ray of Al K_α,1486.6 eV) at SUT-NANOTEC-SLRI joint research facility, Synchrotron Light Research Institute (SLRI), Thailand. The binding energies drift due to charging effects were corrected using the position of the C1s as a reference at 284.8 eV [7,8]. Agilent UV–Vis–NIR spectrophotometer modeled Carry 5000 was used for optical diffuse reflectance spectroscopy (DRS). The diffuse reflectance (%R) spectra were recorded in the wavelength range of 200–2000 nm with the double beam mode. Band gap energy was obtained by extrapolation of the plot of $(Kh\nu)^{1/2}$ versus photon energy ($h\nu$), where K is reflectance transformed according to Kubelka–Munk function [$K = (1 - R)^2/2(R)$]. In this function, $R = (\%R_{sample}/\%R_{standard})$ [9,10]. The electrical conductivities of all sintered samples were measured from 300 to 673 K by four-probe method using a Keysight B2901A source/measure unit.

3. Calculations

The density of states (DOS) were calculated based on density functional theory (DFT) using the Vienna *ab initio* simulation package (VASP) [11,12] employing the Perdew, Burke, Ernzerhof (PBE) exchange-correlation function [13] implemented with the projector augmented-wave method (PAW) [14,15]. Γ-centered $3 \times 3 \times 2$ Monkhorst-Pack k-mesh was used for the Brillouin zone integrations. The cutoff energy for plane-wave basis sets was set at 520 eV. Structural relaxation was performed until the force on each ion is less than 0.01 eV/Å.

4. Results and discussions

4.1. Structure

Powder X-ray diffraction patterns indicate that all samples are single phase (Fig. 1). All diffractions can be indexed as AB_2O_6 defect cubic pyrochlore structure (β-pyrochlore) with $Fd\bar{3}\ m$ space group [16]. The defect pyrochlore structure can be explained based on the interpenetrating network of $(Al,Te)_2O_6$ corner sharing octahedral

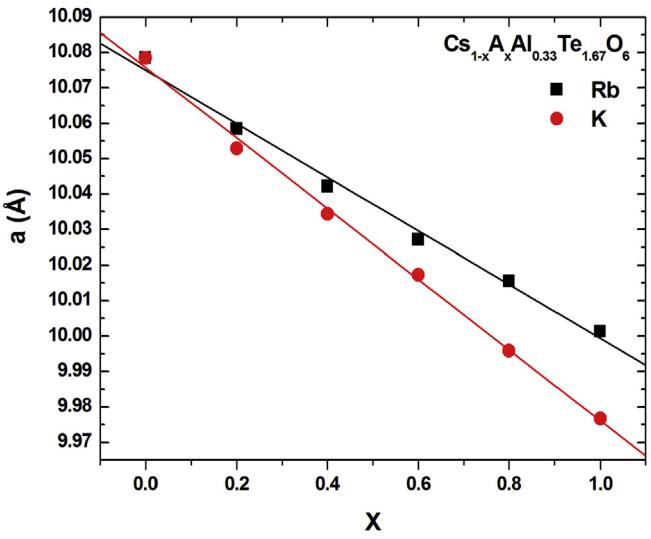

Fig. 2. Plots of cell parameters versus Rb and K content.

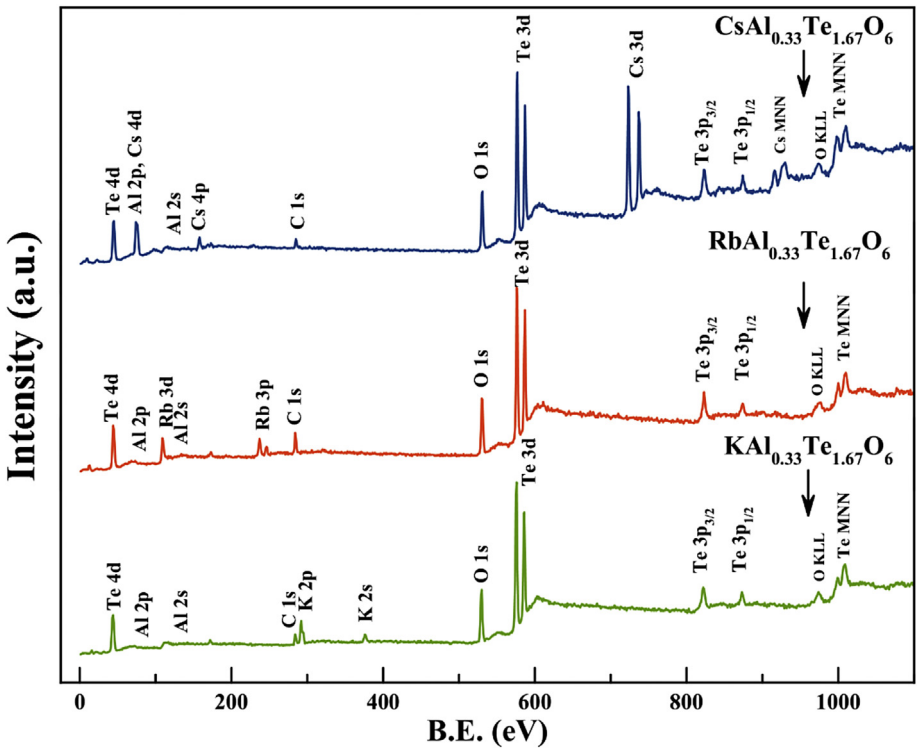

Fig. 3. XPS survey spectra of $CsAl_{0.33}Te_{1.67}O_6$, $RbAl_{0.33}Te_{1.67}O_6$, and $KAl_{0.33}Te_{1.67}O_6$.

units with A cations (Cs, Rb, and K) occupying the interstitial sites. Comparing to $A_2B_2O_7$ pyrochlore, defect pyrochlore structure has lots of vacancies. In addition, there are few possible crystallographic sites for A cations. The XRD patterns in this work suggest no indication of them being at positions other than the normal 8b but small deviation from this ideal position, like the 32e position, is possible.

It is worth to note that the displacive disorder of A cation from 8b to 32e position results in a nonlinear increase of cell parameters in $AAl_{0.33}W_{1.67}O_6$; A = Cs, Rb, and K [17]. However, such anomaly is not observed in this work although the samples are quite similar. Plots of calculated cell parameters versus substituting contents are linear in both series (Fig. 2). As both K^+ (1.51 Å) and Rb^+ (1.61 Å) are smaller than Cs^+ (1.74 Å), increasing their contents results in

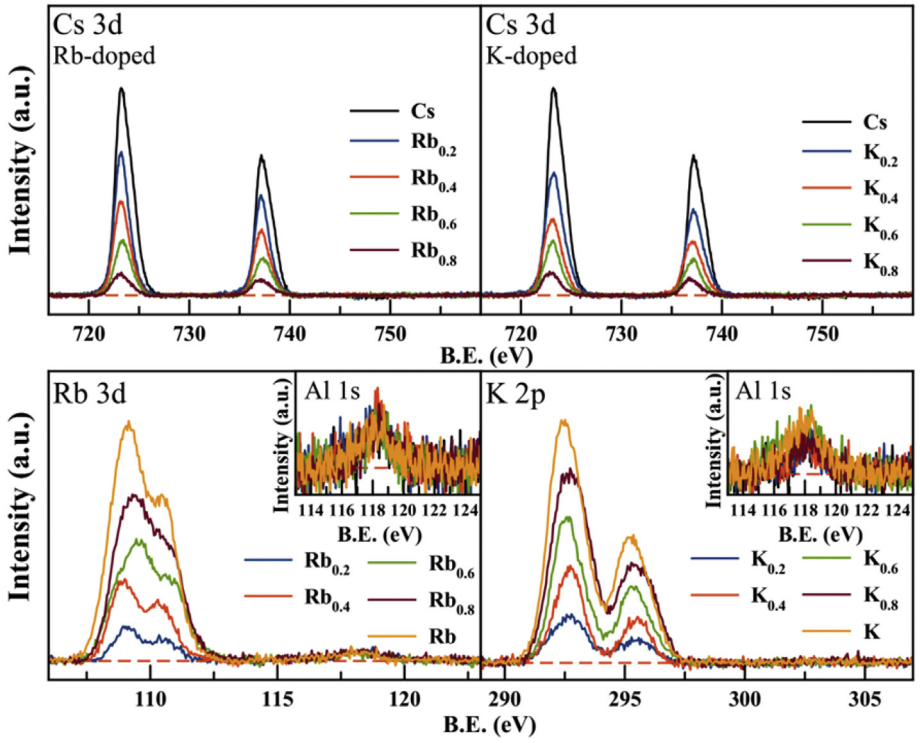

Fig. 4. Cs 3d, Rb 3d, K 2p and Al 1s XPS spectra of $Cs_{1-x}Rb_xAl_{0.33}Te_{1.67}O_6$ and $Cs_{1-x}K_xAl_{0.33}Te_{1.67}O_6$.

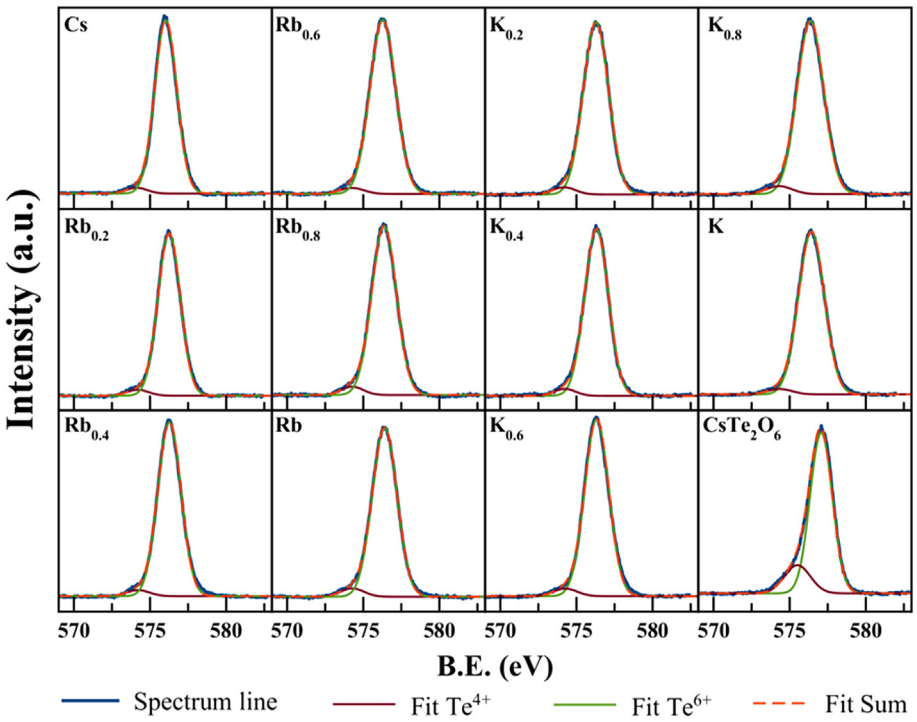

Fig. 5. XPS Te $3d_{5/2}$ spectra of the samples.

smaller cell parameters as expected [18,19]. However, the main network of the structure is the B_2O_6 octahedral network, changing A cations has a much smaller effect on the cell parameters comparing to changing the B cations. Similar results were reported by Castro and Rasines [20].

4.2. XPS results

XPS survey spectra of $CsAl_{0.33}Te_{1.67}O_6$ (CATO), $RbAl_{0.33}Te_{1.67}O_6$ (RATO), and $KAl_{0.33}Te_{1.67}O_6$ (KATO) show the corresponding elemental compositions in each compound (Fig. 3). Cs 3d, Rb 3d and K 2p XPS spectra in Fig. 4 give semi-quantitative results on the composition of the prepared samples. The obtained binding energies are close to those reported in the literature [21-24]. Peak areas of each element in the samples are proportional to the nominal composition.

Table 1
Te $3d_{5/2}$ fitting results.

Comp. (X)	Te^{6+}		Te^{4+}		Ratio of Te^{6+}: Te^{4+} (1.67)	R^2
	B.E. (eV)	FWHM (eV)	B.E. (eV)	FWHM (eV)		
0	576.03	1.70	574.12	1.62	1.62:0.05	0.9983
Rb-doped						
0.2	576.25	1.72	574.19	1.68	1.61:0.06	0.9991
0.4	576.27	1.79	574.22	1.78	1.62:0.05	0.9987
0.6	576.28	2.00	574.25	1.86	1.62:0.05	0.9994
0.8	576.36	1.90	574.28	1.68	1.60:0.07	0.9992
1.0	576.40	1.85	574.28	1.80	1.60:0.07	0.9995
K-doped						
0.2	576.28	1.89	574.29	1.68	1.61:0.06	0.9993
0.4	576.32	1.79	574.33	1.72	1.60:0.07	0.9995
0.6	576.32	1.84	574.34	1.61	1.60:0.07	0.9982
0.8	576.35	2.02	574.43	1.99	1.60:0.07	0.9987
1.0	576.42	1.97	574.46	1.87	1.61:0.06	0.9992
$CsTe_2O_6$						
_	577.07	1.72	575.50	2.00	1.66:0.44 (Te6+1.5: Te4+0.5)	0.9981

XPS spectra of Te $3d_{5/2}$ were also examined to probe oxidation states of Te in the samples. As seen in Fig. 5, all spectra show small asymmetry with a tail on the lower energy region. These spectra were fitted using two Gaussian-Lorentzian peaks; one represents Te^{4+} at lower binding energy and the other represents Te^{6+}. For comparison, Te$3d_{5/2}$ spectra of $CsTe_2O_6$ (CTO), a known compound which contains both $Te^{4+}$and Te^{6+}, are also shown and fitted with the same method here. The binding energy and peak area of each peak are summarized in Table 1. It is interesting to note that while the binding energies of the observed Te^{6+} are close to the reported values, those of Te^{4+} in $Cs_{1-x}A_xAl_{0.33}Te_{1.67}O_6$ (A = K, Rb, and Cs) are slightly smaller than most reported values for Te^{4+} [25,26]. On the other hand, the obtained values are too high to be assigned to Te(0) or Te^{2-} states [27]. As chemical environments affect the binding energy, the binding energy of Te^{4+} in these samples which is in the unique compressed octahedra is expected to be different from that of Te^{4+} in TeO_2 standard. In fact, our values are close to that reported in $Gd_2(Ti_{2-y}Te_y)O_7$ pyrochlores [28].

It is difficult to quantitatively conclude the amount of Te^{4+} in the samples based solely on the peak areas. Nevertheless, the existence of $Te^{4+}$is obvious and its amount in the cubic pyrochlore samples is very low. The presence of small amount of Te^{4+} is a result of small deviation in stoichiometry as reported by Li et al. [6] who concluded that the composition of the prepared $CsAl_{0.33}Te_{1.67}O_6$ was actually $CsAl_{0.30}Te_{1.70}O_6$. A small amount of Te^{6+} must then be reduced to Te^{4+} to maintain charge neutrality. Te $3d_{5/2}$ XPS results reported here reveal the existence of Te^{4+} in all samples with similar peak areas suggesting that the Rb and K substituted samples contain similar defects with a similar amount.

XPS spectra at valence band region (Fig. 6a) give useful information regarding the electronic structure of the samples. Like most oxides, the top of the valence band is predominantly O 2p. The outstanding feature of the spectra is the position of alkali p orbitals

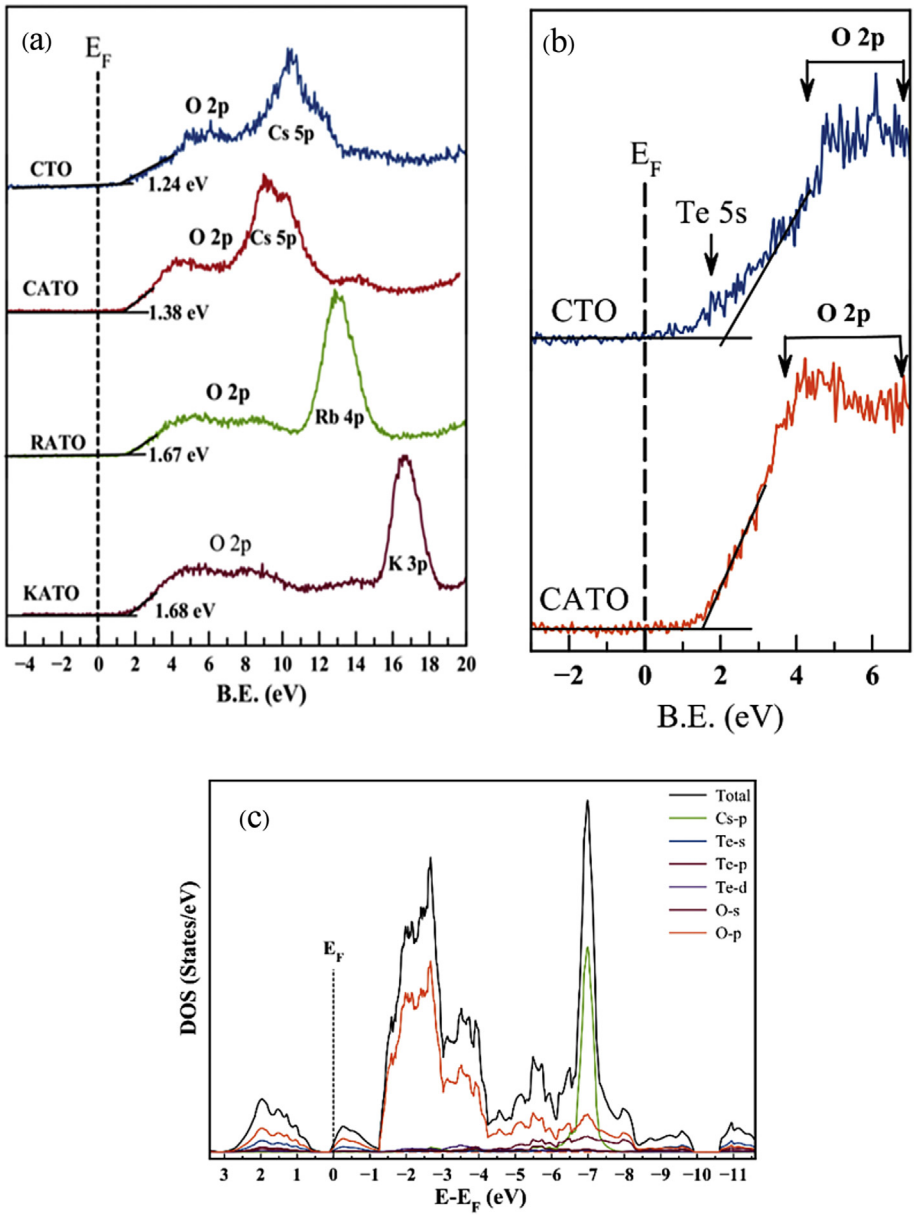

Fig. 6. XPS valence band spectra of $CsTe_2O_6$ and $AAl_{0.33}Te_{1.67}O_6$ (A = Cs, Rb, and K) (a) and the close-up of Cs containing samples showing an additional small peak near the Fermi level (b). (c) shows the calculated valence band of $CsTe_2O_6$.

which is at about 10, 13, and 17 eV for Cs 5p, Rb 4p, and K 3p, respectively. The positions of these states are similar to values in other reports [24,29,30]. Rb 4p and K 3p bands are quite separated from O 2p near the top of the valence band and should not have much contribution in it. Thus, the spectral feature and position of the valence band in Rb and K containing samples are very similar. This also implies that any effects from the difference in bond distances and angles are insignificant. Two samples containing Cs have similar spectra although there are some differences as both samples contain quite a different composition and have related, but different, crystal structure. As Cs 5p bands are clearly overlapping with O2p, Cs is believed to contribute to the valence band. The overlapping between Cs 5p and O 2p in the valence band is observed in many oxides [31,32]. The contribution from Cs 5p broadens the valence band thus causes the shift in its position comparing to the other two samples with no Cs. In addition, the spectral shape of CTO valence band is different from others. Besides the dominant peaks contributed by O 2p, there is another small peak on top of the valence band maximum (VBM) (Fig. 6b).

To gain deeper understandings, band structure calculation was performed for CTO. The valence band of CTO may be divided into three regions (Fig. 6c). The small peaks at VBM consist of O 2p and Te 5s orbitals. The wide region at approximately −1 to −6 eV is predominantly O 2p with a small contribution from Te 4d orbital and the sharp peak at about −6 to −8 eV is formed mainly by Cs 5p orbital with some contribution from Te 5p. These main features of the valence band are qualitatively comparable to the obtained XPS spectra. It is interesting to note that the small peak at VBM is not observed in XPS spectra of the $AAl_{0.33}Te_{1.67}O_6$ series. However, as proposed by Li et al. [6] and deduced from Te $3d_{5/2}$ spectra, $AAl_{0.33}Te_{1.67}O_6$ samples should contain only about 3% of Te^{4+} which is very little comparing to 25% in CTO. Besides, it is difficult to

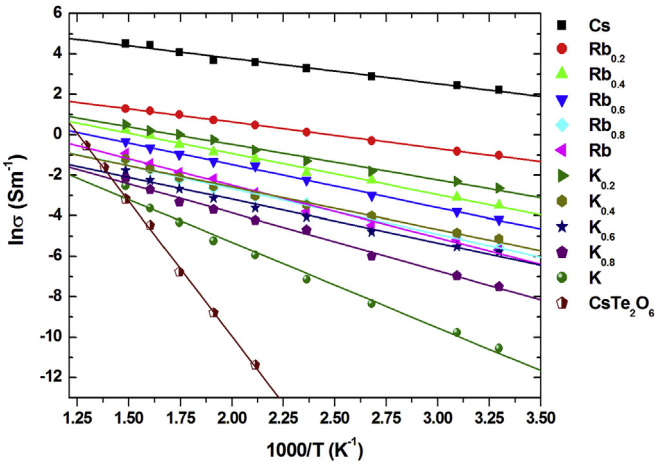

Fig. 7. Electronic conductivities of $Cs_{1-x}A_xAl_{0.33}Te_{1.67}O_6$ (A = Rb and K) and $CsTe_2O_6$ samples fitted with Arrhenius equation.

Table 2
Activation energy and R^2 obtained from fitting the electronic conductivities of $Cs_{1-x}A_xAl_{0.33}Te_{1.67}O_6$; A = Rb and K and $CsTe_2O_6$ with Arrhenius equation.

x	E_a (eV)	R^2	x	E_a (eV)	R^2
0	0.108	0.9854	$CsTe_2O_6$	1.15	0.9987
Rb-doped			**K-doped**		
0.2	0.113	0.9985	0.2	0.151	0.9914
0.4	0.174	0.9921	0.4	0.180	0.9856
0.6	0.183	0.9972	0.6	0.186	0.9855
0.8	0.194	0.9919	0.8	0.247	0.9934
1.0	0.224	0.9870	1.0	0.364	0.9888

compare the spectra of these two series as they have a different structure which leads to the different position of Te 5s.

4.3. Electrical properties

Electronic conductivities of $Cs_{1-x}A_xAl_{0.33}Te_{1.67}O_6$, A = Rb and K decrease with increasing A content. The effect is very significant as room temperature conductivity of $KAl_{0.33}Te_{1.67}O_6$ and $RbAl_{0.33}Te_{1.67}O_6$ are 10^3 and 10^5 times lower than that of $CsAl_{0.33}Te_{1.67}O_6$, respectively (Fig. 7). The conductivities of all samples are plotted based on Arrhenius' equation: $\sigma = Ae^{(-Ea/kT)}$ where A is pre-exponential constant, k is Boltzmann constant, Ea is activation energy, and T is absolute temperature (Fig. 7) and the activation energies are calculated and summarized in Table 2. It is obvious that the lower Cs content, the higher the activation energy. Interestingly, Siritanon et al. [5] previously reported that the Arrhenius plot of $Cs(M,Te)_2O_6$ are not linear in the temperature range 50–300 K and concluded that the samples exhibit variable range hopping conduction as the plots of log conductivity vs. $1/T^{1/4}$ are linear. Therefore, the samples have different conduction mechanisms at different temperatures. In fact, crossover from variable range hopping conduction to thermally activated band conduction from low to high temperatures have been reported in many systems and believed to also be the case here [33,34].

4.4. Optical property

The UV–Vis absorption spectra of $CsTe_2O_6$ and $AAl_{0.33}Te_{1.67}O_6$, A = Cs, Rb, and K are shown in Fig. 8a and the band gap energies obtained from the extrapolations (Fig. 8b) are summarized in Fig. 9. Although most oxides containing Cs and Te have large band gap and white color, the band gap of $CsTe_2O_6$ is only about 1.4 eV and the compound is dark brown. The unusually small band gap is a result of Te^{4+}, Te^{6+} intervalence charge transfer (IVCT) which gives rise to the absorption in a visible region corresponding to the transition from Te^{4+} $5s^2$ to Te^{6+} $5s^0$. Although there are very few reports on Te^{4+}/Te^{6+} charge transfer, a similar mechanism is widely studied in other mixed valence systems including those with post-transition cations like Sb, Sn, Tl [35,36].

UV–Vis spectra of $AAl_{0.33}Te_{1.67}O_6$ series are obviously different from that of $CsTe_2O_6$ although the compounds also contain Te^{4+}/Te^{6+} mixed valency. However, Te^{4+} and Te^{6+} in $CsTe_2O_6$ are in different crystallographic sites while those in $AAl_{0.33}Te_{1.67}O_6$ are in the same one. As λ_{max} of absorption should be directly related to the energy difference between Te^{4+} $5s^2$ and Te^{6+} $5s^0$, the similar environment around Te^{4+} and Te^{6+} in $AAl_{0.33}Te_{1.67}O_6$ results in absorptions at longer wavelengths. Therefore, it is concluded here that the very broad and strong absorption centering at long wavelengths is associated with IVCT of Te^{4+} and Te^{6+}. Mizoguchi et al. [35] also reported similar diffuse reflectance spectra of $BaSn_{1-x}Sb_xO_3$ which contain mixed valence ions and show a very

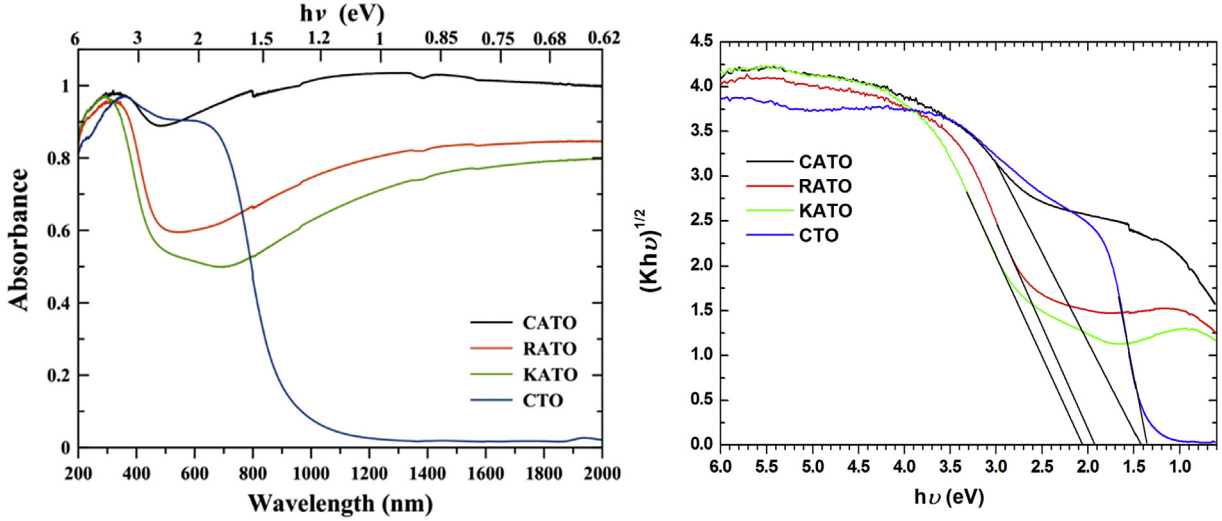

Fig. 8. UV–Vis spectra (a) and extrapolation of the band gap energy (b) of $CsTe_2O_6$ and $AAl_{0.33}Te_{1.67}O_6$ (A = Cs, Rb, and K).

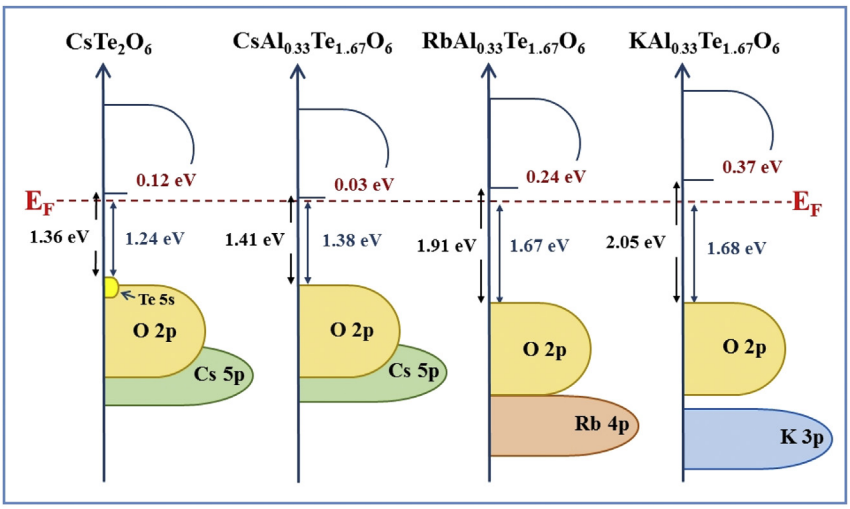

Compounds	Valence band position (eV)	Band gap energy (eV)	E_d (eV)	Activation energy of conduction (eV)
$CsTe_2O_6$	1.24	1.36	0.12	1.15
$CsAl_{0.33}Te_{1.67}O_6$	1.38	1.41	0.03	0.108
$RbAl_{0.33}Te_{1.67}O_6$	1.67	1.91	0.24	0.224
$KAl_{0.33}Te_{1.67}O_6$	1.68	2.05	0.37	0.364

Fig. 9. Schematic band structures of $CsTe_2O_6$ and $AAl_{0.33}Te_{1.67}O_6$ (A = Cs, Rb, and K).

broad absorption band due to IVCT.

5. Discussion

It has been established that $CsAl_{0.33}Te_{1.67}O_6$ shows relatively high conductivity [5]. Li et al. [6] concluded that the conductivity comes from small deviations from stoichiometry which results in small amount of Te^{4+} producing mixed valence compounds. The n-type behavior in these series of compounds is explained by the presence of donor defect levels originating from Te^{4+}. In general, type of M cations in $Cs(M,Te)_2O_6$ affects the conductivities of the compounds as small M cation reduces M/Te-O distance thus destabilizes Te^{4+} in the structure increasing their energy level. In addition, some M cations could provide orbitals with appropriate energy to overlap with Te 5s which increase the conductivity.

When Cs is replaced by Rb and K in $Cs_{1-x}A_xAl_{0.33}Te_{1.67}O_6$, the difference in conductivity is very pronounced although the same Al is present. Additionally, samples containing Rb and K have much lower conductivities despite the smaller cell parameters. XPS results obtained in this work do not indicate any difference in the number of Te^{4+}, hence the number of defect levels, in all samples. In addition, we have also prepared and measured the conductivities of $CsAl_xTe_{2-x}O_6$ and $RbAl_xTe_{2-x}O_6$ with different x values. As shown in Fig. S1 (Supporting Information), the conductivities of both series exhibit similar Al content dependency which is also in agreement with the previous work [6]. It is, therefore, reasonable to conclude that the type and the amount of defect, e.g. Te^{4+}, are similar in all samples. If the number of Te^{4+} is similar, then the difference in conductivities must be related toTe^{4+} energy level relative to the conduction band.

Based on the band gap energy obtained from UV–Vis results and the VBM position obtained from XPS valence band spectra, we propose schematic band structure diagrams of the samples as depicted in Fig. 9. From the figure, the difference between Fermi energy level and the bottom of the conduction band (E_d) is obtained. Generally, the band diagrams of these four samples represent their semiconducting behavior. However, the activation energies of conduction indicate that their behaviors are different. The activation energy of conduction of $CsTe_2O_6$ (1.15 eV, Fig. 7) is in the same order with its band gap energy suggesting the intrinsic semiconducting behavior. The conductivity of this sample is small because large energy is required to activate electrons across the band gap. It is noteworthy that E_d and the activation energy of conduction in $CsTe_2O_6$ are significantly different which indicates that there is no defect level at the Fermi energy level (E_F). On the other hand, the activation energies of $AAl_{0.33}Te_{1.67}O_6$ are close to E_d and much smaller than their band gap energy which suggests the presence of defect levels close to the conduction band within the band gap. The presence of such defect levels is a characteristic of n-type semiconductors which agrees well with the negative Seebeck coefficients [5]. E_d in these three samples indicate the position of defect levels relative to conduction band minimum (CBM) which determines conductivities of the samples.

Replacing Cs with Rb and K have two effects on the band diagram; lowering the VBM and increasing the band gap energy. It should be noted that lowering VBM in these cases is not the only cause of increasing the band gap. Without the presence of Cs, VBM of both $RbAl_{0.33}Te_{1.67}O_6$ and $KAl_{0.33}Te_{1.67}O_6$ are about 0.3 eV lower in energy. However, the band gap differences between the samples are 0.5–0.6 eV. As the conduction band should be mainly Te 5s with some contribution from Al and O, Te/Al-O bond distance and Te/Al-O-Te/Al bond angle must play important roles in determining the CBM. Additional detail studies are required to further explain this matter. Nevertheless, the combination of VBM lowering and the

increase in band gap energy when Cs is replaced with Rb and K result in larger E_d and consequently lower conductivity.

6. Conclusions

Series of $AAl_{0.33}Te_{1.67}O_6$ (A = Cs, Rb, and K) with pyrochlore structure have been prepared by solid state reaction and their electronic properties have been characterized. Electrical conductivities of the compounds arise from small deviation from stoichiometry which results in Te^{4+}/Te^{6+} mixed valency as evidenced in XPS results. Although containing similar Te^{4+}/Te^{6+} mixed valency, the samples with Rb and K are significantly less conductive. Based on the obtained XPS at valence band region, optical band gap energy, and activation energy of conduction; the band diagrams are proposed and used to explain the large difference in electrical conductivities. The band diagrams indicate that the samples are n-type semiconductor. The energy difference between CBM and donor states which determines the conductivity is affected by A cations. Replacing Cs with Rb and K increases this energy difference which consequently results in the lower electrical conductivity.

Acknowledgements

This work is financially supported by The Thailand Research Fund and Suranaree University of Technology, Thailand (Grant No. TRG5780068). We thank the synchrotron light research institute (public organization), Thailand, especially SUT-NANOTEC-SLRI joint research facility, for XPS facilities. We also gratefully acknowledge S. Jungthawan for useful discussions on calculation methods. T. Kongnok acknowledges financial support from the Thailand Research Fund and Suranaree University of Technology (Grant No. IRG5780010).

Appendix A. Supplementary data

Supplementary data related to this article can be found at http://dx.doi.org/10.1016/j.jallcom.2017.05.025.

References

[1] H. Kawazoe, H. Yanagi, K. Ueda, H. Hosono, Mrs Bull. 25 (2000) 28–36.
[2] S. Noguchi, H. Sakata, J. Phys. D. Appl. Phys. 13 (1980) 1129.
[3] S. Cai, Y. Li, X. Chen, Y. Ma, X. Liu, Y. He, J. Mater. Sci. Mater. Electron 27 (2016) 6166–6174.
[4] D.H. O'Neil, V.L. Kuznetsov, R.M. Jacobs, M.O. Jones, P.P. Edwards, Mater. Chem. Phys. 123 (2010) 152–159.
[5] T. Siritanon, G. Laurita, R.T. Macaluso, J.N. Millican, A.W. Sleight, M. Subramanian, Chem. Mater. 21 (2009) 5572–5574.
[6] J. Li, T. Siritanon, J.K. Stalick, A.W. Sleight, M. Subramanian, Inorg. Chem. 50 (2011) 5747–5754.
[7] W.-Y. Howng, R. Thorn, J. Phys. Chem. Solids 41 (1980) 75–81.
[8] Y. Lv, W. Yao, R. Zong, Y. Zhu, Sci. Rep. 6 (2016).
[9] R. Guje, G. Ravi, S. Palla, K.N. Rao, M. Vithal, Mater. Sci. Eng. B 198 (2015) 1–9.
[10] A.E. Morales, E.S. Mora, U. Pal, Rev. Mex. Fis. S 53 (2007) 18.
[11] G. Kresse, J. Hafner, Phys. Rev. B 48 (1993) 13115.
[12] F. Fuchs, J. Furthmüller, F. Bechstedt, M. Shishkin, G. Kresse, Phys. Rev. B 76 (2007) 115109.
[13] J.P. Perdew, K. Burke, M. Ernzerhof, Phys. Rev. Lett. 77 (1996) 3865.
[14] P.E. Blöchl, Phys. Rev. B 50 (1994) 17953.
[15] G. Kresse, D. Joubert, Phys. Rev. B 59 (1999) 1758.
[16] M. Subramanian, G. Aravamudan, G.S. Rao, Prog. Solid State Chem. 15 (1983) 55–143.
[17] G.J. Thorogood, B.J. Kennedy, V.K. Peterson, M.M. Elcombe, G.J. Kearley, J.V. Hanna, V. Luca, J. Solid State Chem. 182 (2009) 457–464.
[18] R.T. Shannon, C.T. Prewitt, Acta Crystallogr. B 25 (1969) 925–946.
[19] R.T. Shannon, Acta Crystallogr. A 32 (1976) 751–767.
[20] A. Castro, I. Rasines, X. Turrillas, J. Solid State Chem. 80 (1989) 227–234.
[21] R. Marschall, A. Mukherji, A. Tanksale, C. Sun, S.C. Smith, L. Wang, G.Q.M. Lu, J. Mater. Chem. 21 (2011) 8871–8879.
[22] C. Guo, S. Yin, Q. Dong, T. Sato, CrystEngComm 14 (2012) 7727–7732.
[23] G. Ravi, N.K. Veldurthi, S. Palla, R. Velchuri, S. Pola, J.R. Reddy, M. Vithal, Photochem. Photobiol. 89 (2013) 824–831.
[24] V. Atuchin, V. Kesler, G. Meng, Z. Lin, J. Phys. Condens. Matter 24 (2012) 405503.
[25] M. Sathiya, K. Ramesha, G. Rousse, D. Foix, D. Gonbeau, K. Guruprakash, A. Prakash, M. Doublet, J.-M. Tarascon, Chem. Commun. 49 (2013) 11376–11378.
[26] G. Tan, X. Zhang, Z. Chen, J. Appl. Phys. 95 (2004) 6322–6324.
[27] W.E. Sartz Jr., K.J. Wynne, D.M. Hercules, Anal. Chem. 43 (1971) 1884–1887.
[28] A. Heredia, M.Q. García, J.P. Mazariego, R. Escamilla, J. Alloy Compd. 504 (2010) 446–451.
[29] B. Slobodin, L. Surat, V. Zubkov, A. Tyutyunnik, I. Berger, M. Kuznetsov, L. Perelyaeva, I. Shein, A. Ivanovskii, B. Shulgin, Phys. Rev. B 72 (2005) 155205.
[30] S. Van den Berghe, J.-P. Laval, B. Gaudreau, H. Terryn, M. Verwerft, J. Nucl. Mater. 277 (2000) 28–36.
[31] S.B. Waghmode, R. Vetrivel, S.G. Hegde, C.S. Gopinath, S. Sivasanker, J. Phys. Chem. 107 (2003) 8517–8523.
[32] Y. Yang, X. Su, S. Pan, M. Zhang, Y. Wang, J. Han, Z. Yang, CrystEngComm 16 (2014) 1978–1984.
[33] M. Han, K. Jiang, J. Zhang, W. Yu, Y. Li, Z. Hu, J. Chu, J. Mater. Chem. 22 (2012) 18463–18470.
[34] M. Okutan, H.I. Bakan, K. Korkmaz, F. Yakuphanoglu, Phys. B Condens. Matter 355 (2005) 176–181.
[35] H. Mizoguchi, P. Chen, P. Boolchand, V. Ksenofontov, C. Felser, P.W. Barnes, P.M. Woodward, Chem. Mater. 25 (2013) 3858–3866.
[36] L. Atkinson, P. Day, J. Chem. Soc. A (1969) 2423–2431.